A STUDY OF THE TRANSIENT MAGNETIC FIELD IN IRON AND SIMPLE RELATIONS FOR NUCLEAR MOMENTS

PROEFSCHRIFT

TER VERKRIJGING VAN DE GRAAD VAN DOCTOR IN DE WISKUNDE EN NATUURWETENSCHAPPEN AAN DE RIJKSUNIVERSITEIT TE UTRECHT, OP GEZAG VAN DE RECTOR MAGNIFICUS PROF. DR. A. VERHOEFF, VOLGENS BESLUIT VAN HET COLLEGE VAN DECANEN IN HET OPENBAAR TE VERDEDIGEN OP WOENSDAG 30 NOVEMBER 1977 DES NAMIDDAGS TE 4.15 UUR

door

PETER CORNELIS ZALM
geboren op 16 januari 1951
te Eindhoven

PROMOTOR: PROF.DR. P.M. ENDT

Dit proefschrift kwam tot stand mede onder leiding van:

DR. P.W.M. GLAUDEMANS (theorie)

DR. G. VAN MIDDELKOOP (experiment)

Voor mijn vrienden

Typewerk : Monique de la Bey
Diet Bos
Tekeningen: Hilde Elberse
Drukwerk : Elinkwijk b.v., Utrecht

CONTENTS

INTRODUCTION AND SUMMARY vii

PART A (THEORY)

CHAPTER

I SIMPLE RELATIONS FOR NUCLEAR MOMENTS (I) 3
(magnetic dipole moments in the shell-model picture)
1. Introduction 3
2. The additivity relation 4
3. Isoscalar and isovector parts of the g-factor 9
4. Comparison with experiment 12
5. Conclusions 19

II SIMPLE RELATIONS FOR NUCLEAR MOMENTS (II) 23
(electric quadrupole moments of quasi-rotational states in even-even nuclei)
1. Introduction 23
2. Derivation of the relations 24
3. Comparison with experiment 28
4. Additional remarks and conclusions 32

PART B (EXPERIMENT)

III THE USE OF SINGLE CRYSTAL IRON FRAMES IN TRANSIENT FIELD EXPERIMENTS 41
1. Introduction 41
2. Magnetization of the ferromagnetic backing 42
3. Surface magnetization measurements 43
4. Application to transient field IMPAC measurements 50
5. Conclusion 56

IV VELOCITY AND ATOMIC NUMBER DEPENDENCE OF THE TRANSIENT MAGNETIC FIELD IN IRON 59

1. Introduction 59
2. Experimental procedure and results 60
3. Systematics of the transient magnetic field in Fe... 63
4. A microscopic interpretation 68
5. Conclusions and summary 74

V TRANSIENT FIELD g-FACTOR MEASUREMENTS ON THE 2_1^+ STATES OF ^{32}S AND ^{34}S 80

1. Introduction 80
2. Experimental procedure 81
3. Statistical considerations, analysis and results.... 82
4. Comparison with theory and conclusion 86

SAMENVATTING 90

CURRICULUM VITAE 92

INTRODUCTION AND SUMMARY

The nuclear structure studies performed in our laboratory are characterized by a strong interaction between theory and experiment. Large-scale shell-model calculations are tested against spectroscopic information such as spins, parities, lifetimes and γ-ray decay of excited states of (mainly) sd-shell nuclei. Since 1972 also static magnetic dipole moments of excited states are investigated experimentally in our laboratory through magnetic hyperfine interaction studies. In this thesis theoretical and experimental studies on nuclear moments are described.

In the first two chapters (part A) some simple theoretical relations for magnetic dipole and electric quadrupole moments are presented. The relations are simple in the sense that the underlying theoretical models provide a simple picture which can be understood relatively easily. They are also simple because they require only "back-of-the-envelope" calculations. Quantities that would require complex model-dependent estimates or large-scale computer calculations are replaced by experimental observables or crude simple-model estimates.

In chapter I g-factors (i.e. the ratio of the magnetic dipole moment and spin of a nuclear state) are discussed. As a starting point the nucleus is described by the shell model. In this model most nucleons form an inert core which creates a central field in which only a few (outer) nucleons move. These active particles determine the properties of the nucleus. First the additivity relation for g-factors of neighbouring nuclei is discussed. Next the separation of g-factors into an isoscalar and an isovector part is used to study nuclei with atomic mass $A \leq 55$. The results of calculations with these relations are compared with experimentally known g-factors and a good agreement is found.

In the second chapter electric quadrupole moments of quasi-rotational states in even-even nuclei are studied. Here a collective model is used to describe the nuclear properties. In this model a deformed nucleus is taken to consist of two parts, an inner superfluid core, which does not participate in the collective motion,

plus an outer fluid, which moves bodily about it. Such a description is the collective analogon of the individual-particle shell-model. It is shown that within the limits of this "rotationally invariant core" model there is a relation between the quadrupole moment and the excitation energy of a rotational state. This relation, which is linear to first order, proves insensitive to the exact form of the nuclear matter density distribution. Calculated values are compared with experimentally known quadrupole moments. For the mass region A = 18-208 good overall agreement is observed.

From the study of such simple relations it becomes clear that in many cases, mostly for low-lying states, nuclear moments can be estimated with reasonable accuracy from crude model assumptions together with other experimental information. One should therefore focus attention to states whose moments are more sensitive to model parameters. These states are generally higher excited and hence often short-lived. This necessitates the development of sophisticated techniques. In the second part (B) of this thesis an experimental technique for measuring g-factors of short-lived states (τ_m = 0.1-10 ps) is discussed. In this method one uses the strong hyperfine interaction caused by the transient magnetic field. Such a field is experienced by nuclei during their recoil into magnetized ferromagnetic media. By this interaction of the field with the magnetic dipole moment of an excited state the nucleus precesses. This is observed as a rotation of the angular distribution of γ-rays emitted in the decay of that state. The transient field method dates from 1967. It has been applied and extended to light nuclei and short lifetimes in our laboratory previous to the present work. By improving the experimental technique (chapter III) the calibration of the transient field in iron (chapter IV) was facilitated after it had become clear that these fields deviate appreciably from the commonly accepted description. This calibration has also led to a better understanding of the atomic nature of the transient field phenomenon itself.

In chapter III we show that a gain in measuring time of at least a factor of four can be obtained by the use of a single crystal iron frame as a ferromagnetic target backing in which the excited

nuclei, formed in a nuclear reaction, recoil. Such frames can be fully magnetized with low external fields as shown by magneto-optical Kerr-effect measurements. The important improvement is that the associated magnetic fringing field near the target is negligible. This is in contrast to the conventional set-up in which strong external fields, with corresponding large disturbing fringing fields, were necessary. The single-crystal set-up is compared to the conventional set-up in several transient field experiments and proves to be successful.

Next, in chapter IV, the transient field phenomenon itself is studied. The dynamical behaviour of this field must be known in order that g-factors can be extracted from the measured precessions. In experiments performed previously in our laboratory the measured precession angles were found to increase approximately proportionally with velocity for ^{28}Si in Fe. The associated strong fields (1000 T) at high velocity have been explained by the capture of polarized electrons from the ferromagnetic host into bound atomic s-shells of the moving nuclear ion. In this chapter we describe precession measurements on ^{20}Ne and ^{24}Mg at various velocities (to $v/c \approx 0.06$). These measurements, together with data obtained elsewhere, establish the universality of the linear velocity dependence of the field. In addition a marked structure is observed in the atomic number dependence for light ions in iron. It is shown that the field strength can be parametrized empirically if it is assumed that the field is caused predominantly by unpaired polarized electrons in specific s-shells depending on atomic number.

These observations are discussed within the framework of the microscopic "polarized electron capture" model (see above). This model can at least qualitatively account for the empirically obtained velocity and atomic number dependences. The "saw-tooth" like atomic number dependence, an atomic shell effect, can be correlated with the formation of quasimolecules in collisions of the moving ion with the host (Fe) atoms.

In chapter V, finally, an application of the experimental method is described. With the field calibration given in chapter IV the g-factors of the first-excited 2^+ states of ^{32}S and ^{34}S are determined

from the observed precessions. A comparison with theoretical predictions indicates that the transient field calibration is satisfactory.

This work was performed as part of the research programme of the "Stichting voor Fundamenteel Onderzoek der Materie" (FOM) with financial support from the "Nederlandse Organisatie voor Zuiver-Wetenschappelijk Onderzoek" (ZWO).

PART A (THEORY)

CHAPTER I

SIMPLE RELATIONS FOR NUCLEAR MOMENTS (I)
(magnetic dipole moments in the shell-model picture)

1. Introduction

In this chapter some methods and formulae are discussed to estimate nuclear g-factors of low-lying states. The shell-model picture is used in the derivation of all expressions presented here. Rather than attempting to give elaborate theoretical calculations of the quantities entering in the expressions, we shall replace them by experimental observables or by estimates obtained under simplifying assumptions, such as pure j^n configurations and charge symmetry of the nuclear forces.

Some of the resulting relations between experimental observables have been discussed previously (see e.g. [1-3]), sometimes in a different presentation. As in the mean time considerably more experimental information has become available, a better test of their applicability can now be made. It is also important to know the reliability of the g-factor estimates that are obtained with the simple relations discussed here, in particular for the calibration of experimental techniques for g-factor measurements. The latter concern, for instance, the transient field ion-implantation perturbed angular correlation method, as will be outlined in chapter IV (see also [4]).

First, in sect. 2, the well-known additivity relation for nuclear g-factors is discussed briefly. An empirical method to include large parts of the effects of meson exchange and core polarization is given and a comparison with experiment is made. Next, in sects. 3 and 4, the isoscalar and isovector g-factors are studied separately for the mass region $A \lesssim 56$. Finally, conclusions and consequences of the present analysis are summarized in sect. 5.

2. The additivity relation

2.1. GENERAL REMARKS

Consider a nucleus with angular momentum J to consist of three groups of nucleons, i.e. the core with $J_{core} = 0$ and two groups, to be specified later, labelled 1 and 2 with angular momenta J_1 and J_2. Let the g-factor g_i (i = 1,2) correspond to the system core + group (i). If the interaction between the groups 1 and 2 is neglected, one obtains for the g-factor of the whole nucleus [5]

$$g(J_1 \otimes J_2 = J) = \frac{g_1+g_2}{2} + \frac{g_1-g_2}{2} \cdot \frac{J_1(J_1+1) - J_2(J_2+1)}{J(J+1)} . \qquad (2.1)$$

Equation (2.1) is the well-known additivity relation. It has been used mostly for odd-odd nuclei with a doubly-even core and the groups 1 and 2 taken as one proton and one neutron, respectively [1].

For practical purposes (2.1) is used to relate the experimental g-factors of the nucleus in which both groups are present and the two nuclei which consist of the core plus one group only. Once reasonable assumptions are made about the groups 1 and 2, based on the single-particle shell model and spin/parity considerations, (2.1) provides a useful tool for estimating one of the factors g, g_1 and g_2 if the other two are known. These estimates are necessarily not exact, however, as the effect of the interaction between the groups is not included. This can be partly circumvented though, as will be outlined in the next subsection.

A consequence of (2.1) is that the g-factors for all possible j^n configurations of identical nucleons should be the same. A beautiful example is given by the $1h^n_{9/2}$ proton states outside a ^{208}Pb closed core in ^{209}Bi [$J^\pi = 9/2^-$; g = 0.913], ^{210}Po [6^+; 0.908(4) and 8^+; 0.914(4)], ^{211}At [$21/2^-$; 0.910(6)], ^{212}Rn [8^+; 0.911(12)], ^{213}Fr [$21/2^-$; 0.886(15)] and ^{214}Ra [8^+; 0.901(4)].

Another important implication of (2.1) is that the g-factor of a nucleus with one group of active nucleons outside the core is not

affected by the addition of a group of nucleons coupled to J = 0. This enables us to apply (2.1) also in those cases where the g-factor of one, or both, of the nuclei consisting of core + group (i) (i = 1, 2) has not been measured. One simply takes the known g-factor of the corresponding state in a nucleus with a pair of identical nucleons more or less. Sign assignments are also possible in this way. Throughout this chapter to all experimental g-factors with unknown signs used in the analyses or comparisons, a sign was attributed along this line.

From a compilation of measured nuclear moments [6] it is observed that the g-factors of corresponding states in nuclei with $A \gtrsim 56$ that differ by an even number of protons and/or neutrons, are indeed rather close. For $A \lesssim 56$, however, systematic deviations from this simple rule occur. This may be attributed to the fact that when all valence protons and neutrons are in the same subshell, the internal coupling of e.g. the neutrons is affected by the addition of a pair of protons in that shell. It turns out that the effect of recoupling is smaller when the protons and neutrons are in different shells. The occurrence of all valence nucleons in the same subshell is typical for selfconjugated nuclei and their close neighbours. Hence for $A \lesssim 56$ other methods for estimating the g-factors are given in sects. 3 and 4.

2.2. ATTAINABLE ACCURACY

Let us denote by $({}_{j_p}{}^{z}C^{n}_{j_n})_J$ a system with total angular momentum J, consisting of an inert core C, a group of z valence protons coupled to angular momentum j_p and n neutrons coupled to j_n. As argued in the previous subsection the systems $({}^{2z}_{o}C^{2n+1}_{j_n})$, with varying z and n, should have the same g-factor. The same notion underlies the Schmidt-estimates for g-factors of odd-mass nuclei with one unpaired nucleon in a subshell, nlj,

$$g_{P,N} = g^{l}_{p,n} \pm \frac{g^{s}_{p,n} - g^{l}_{p,n}}{2l+1} \quad \text{for } j = l \pm \tfrac{1}{2}. \tag{2.2}$$

Here the subscripts P and N refer to the odd nucleon being a proton or a neutron and $g_p^l = 1$, $g_n^l = 0$, $g_p^s = 5.586$ and $g_n^s = -3.826$ stand for the single-proton and -neutron spin and orbital g-factors.

In a nucleus many corrections to (2.2) exist that can be classified into three categories. Firstly there are corrections that are roughly constant for a given subshell nlj, as e.g. renormalizations of the bare-nucleon spin and orbital g-factors due to the mesonic exchange currents. Also changes of the predictions of (2.2) as a whole belong to this category, as e.g. effects due to momentum dependent forces such as the two-body $\vec{L}\vec{S}$-force [7]. Secondly there are corrections that are approximately linear in the number of valence protons and neutrons like first-order core polarization or configuration mixing [8]. All nonsystematic changes are taken to fall in the third class.

Slightly generalizing the above remarks, we may write

$$g({}^{2z}_{o}C^{2n+1}_{j_n}) = \frac{1}{2}\{g({}^{2z}_{o}C^{2n-1}_{j_n}) + g({}^{2z}_{o}C^{2n+3}_{j_n})\} + \delta g, \qquad (2.3)$$

where one has $\delta g \simeq 0$ if nonlinear effects are not too important. Of course, relations similar to (2.3) exist with varying z, rather than with varying number of neutrons, as well as for odd-proton nuclei instead of odd-neutron nuclei. Equation (2.3), which is a special case of the additivity relation (2.1), can be thought of as resulting from a Taylor series expansion to first order in the number of valence neutrons (or protons) and δg should then account for all higher-order derivatives. Another, tentative, explanation can be generated by counting the number of $\pi\pi$, $\pi\nu$, $\nu\nu$, πC and νC interactions (π = valence proton, ν = valence neutron, C = core) in all systems involved in (2.3). It shows that only the effect due to two neglected $\nu\nu$ interactions has to be included in δg.

From the nuclear moment compilation [6] it follows that (2.3) and the analogous equations can be tested in some 60 cases with $A > 56$, where all three g-factors in a chain of nuclei connected

through (2.3) have been measured. It is observed that δg is quite small and varies in a nonsystematic way, independent of spin or mass. Hence δg is assumed to be a constant "procedural error" to be added quadratically, i.e. incoherently, to the experimental errors. A conservative estimate of δg can be obtained by variation of δg until a goodness-of-fit of $\chi^2 = 1$ is obtained; i.e. δg has to account for the unexplained residual variance observed in the application of (2.3) to the data. It was found from the (60) experimental data that a value of $\delta g = 0.012$ can thus account for the observed discrepancies.

In case the additivity relation (2.1) is used to estimate the g-factor of the odd-odd nucleus denoted by $({}^{2z+1}_{j_p}C^{2n+1}_{j_n})_J$, the best approach is as follows. The g-factor of e.g. the proton group must be taken as the average over the g-factors of $({}^{2z+1}_{j_p}C^{2n}_{o})$ and $({}^{2z+1}_{j_p}C^{2n+2}_{o})$ and similarly for the neutron group. In the same manner as before, such a procedure can be interpreted as minimization of the number of higher-order derivatives in a Taylor expansion in the number of protons and neutrons. Or, in the alternative explanation, the number of neglected nucleon-nucleon interactions has been minimized. Likewise, for a system like $({}^{o}_{o}C^{2n}_{J})$ the average over the g-factors of $({}^{o}_{o}C^{2n-1}_{j})$ and $({}^{o}_{o}C^{2n+1}_{j})$ must be taken.

In table 1 a comparison is made between experimental g-factors and those obtained with (2.1) and the minimalization methods discussed above. All available nuclei are included, for which a reasonable configuration assignment is possible and of which the g-factors have been measured with an accuracy of better than 10%. The agreement is striking and the observed small discrepancies can be explained, in the same way as before, with a residual "procedural error" of $\delta g = 0.006$. If, for comparison, only the nuclei with either mass A-1 or mass A+1 are used in the g-factor estimate of the mass A nucleus, a residual error of $\delta g = 0.03$ has to be assumed.

Summarizing, we may state that estimates with an uncertainty of about $\delta g \simeq 0.01$ can be obtained from the additivity relation if all g-factors needed for optimum use of (2.1) are available and the division into subgroups is unambiguous. A disadvantage of the minimalization procedure is that many experimental data have to be avail-

Table 1

A comparison between experimental g-factors [a)] and those calculated with the additivity relation following a minimalization procedure (see text)

Nucleus; J^{π}	Assumed configuration	Nuclei used for g_1	Nuclei used for g_2	g_{exp}	g_{add}
^{2}H ; 1^{+}	$\pi s_{1/2}\nu s_{1/2}$	$^{1,3}H$	n, ^{3}He	+0.857	+0.865
^{14}N , 1^{+}	$\pi p_{1/2}\nu p_{1/2}$	$^{13,15}N$	^{13}C, ^{15}O	+0.404	+0.408
^{18}F ; 3^{+}	$\pi d_{5/2}\nu d_{5/2}$	$^{17,19}F$	^{17}O, ^{19}Ne	+0.572(3)	+0.570(1)
^{36}Cl; 2^{+}	$\pi d_{3/2}\nu d_{3/2}^{-1}$	$^{35,37}Cl$	^{35}S, ^{37}Ar	+0.643	+0.576(33)
^{38}K : 3^{+}	$\pi d_{3/2}^{-1}\nu d_{3/2}^{-1}$	$^{37,39}K$	^{37}Ar, ^{39}Ca	+0.458	+0.428(34)
^{40}K , 4^{-}	$\pi d_{3/2}^{-1}\nu f_{7/2}$	$^{39,41}K$	^{39}Ar, ^{41}Ca	-0.325	-0.291(34)
^{40}K : 3^{-}	$\pi d_{3/2}^{-1}\nu f_{7/2}$	$^{39,41}K$	^{39}Ar, ^{41}Ca	-0.43(3)	-0.414(43)
^{42}Ca; 6^{+}	$\nu f_{7/2}^{2}$	$^{41,43}Ca$	$^{41,43}Ca$	-0.415(15)	-0.416
^{50}V : 6^{+}	$\pi f_{7/2}\nu f_{7/2}^{-1}$	$^{49,51}V$	^{49}Ti, ^{51}Cr	+0.558	+0.542(4)
^{54}Fe; 6^{+}	$\pi f_{7/2}^{-2}$	^{53}Mn, ^{55}Co	^{53}Mn, ^{55}Co	+1.37(3)	+1.407(1)
^{112}In; 8^{-}	$\pi g_{9/2}^{-1}\nu h_{11/2}$	$^{111,113}In$	^{111}Cd, ^{113}Sn	+0.385(4)	+0.395(3)
^{114}In; 5^{+}	$\pi g_{9/2}^{-1}\nu s_{1/2}$	$^{113,115}In$	^{113}Cd, ^{115}Sn	+0.94(2)	+0.953
^{122}Sb; 3^{+}	$\pi g_{7/2}\nu s_{1/2}$	$^{121,123}Sb$	^{121}Sn, ^{123}Te	+0.994(4)	+0.994(14)
^{130}I ; 5^{-}	$\pi g_{7/2}\nu h_{11/2}$	$^{129,131}I$	^{129}Te, ^{131}Xe	-0.025(3)	-0.020(8)
^{138}La; 5^{+}	$\pi g_{7/2}^{-1}\nu d_{3/2}^{-1}$	$^{137,139}La$	^{137}Ba, ^{139}Ce	+0.743	+0.733(19)
^{148}Pm; 6^{-}	$\pi g_{7/2}^{-1}(\nu f_{7/2}^{5})_{5/2}$	$^{147,149}Pm$	^{147}Nd, ^{149}Sm	+0.30(3)	+0.315(10)
^{170}Tm; 1^{-}	$\pi s_{1/2}\nu p_{1/2}$	$^{169,171}Tm$	^{169}Er, ^{171}Yb	+0.248(4)	+0.274(13)
^{206}Pb; 12^{+}	$\nu i_{13/2}^{2}$	$^{205,207}Pb$	$^{205,207}Pb$	-0.152(4)	-0.152(4)
^{206}Bi; 10^{-}	$\pi h_{9/2}\nu i_{13/2}$	$^{205,207}Bi$	^{205}Pb, ^{207}Pb	+0.263(2)	+0.268(5)

a) The experimental values stem from [6] and errors smaller than the last digit are not given.

able. On the other hand, many nuclei belong to more than one string of nuclei connected through (2.1).

3. Isoscalar and isovector parts of the g-factor

Under the assumption that mesonic exchange effects are negligible, the magnetic-moment operator can be written in a model-independent way as the sum of single-particle operators [5]

$$\vec{\mu} = \sum_{i=1}^{A} \{\frac{1-\tau_3(i)}{2} [g_p^l \vec{l}(i) + g_p^s \vec{s}(i)] + \frac{1+\tau_3(i)}{2} [g_n^l \vec{l}(i) + g_n^s \vec{s}(i)]\}. \tag{3.1}$$

Here g_p^s, g_n^s, g_p^l and g_n^l stand for the single-proton and -neutron spin and orbital g-factors. The magnetic moment μ is defined as the expectation value of the z-component of $\vec{\mu}$ in the state with a definite value of the spin J and projection M = J; it is given in units of nuclear magneton.

If charge dependence of nuclear forces is neglected, it follows from (3.1) that the magnetic moments of corresponding states in mirror nuclei can be written as $\mu(T_3 = \pm T) = \mu_o \pm \mu_1$ where μ_o is called the isoscalar and μ_1 the isovector magnetic moment. With the operator identity $\sum_{i=1}^{A} \{\vec{l}(i) + \vec{s}(i)\} = \vec{J}$ one obtains from (3.1) for the corresponding parts of the g-factor the relations

$$g_o = \frac{\mu(T_3=+T) + \mu(T_3=-T)}{2J} = \frac{g_n^l+g_p^l}{2} + \frac{g_n^s+g_p^s-g_n^l-g_p^l}{2J} \langle s\rangle \tag{3.2}$$

and

$$g_1 = \frac{\mu(T_3=T) - \mu(T_3=-T)}{2J} = \frac{g_n^l-g_p^l}{2J} \langle \tau j\rangle + \frac{g_n^s-g_p^s-g_n^l+g_p^l}{2J} \langle \tau s\rangle. \tag{3.3}$$

The matrix elements represent a straightforward condensed notation for the expectation values of the z-components of the operators for the state $|J,M = J,T,T_3 = +T\rangle$.

It follows from (3.2) and (3.3), after insertion of free-nucleon spin and orbital g-factors ($g_p^s = 5.586$, $g_n^s = -3.826$, $g_p^l = 1$, $g_n^l = 0$) that fairly accurate estimates for g_o and g_l are obtained with relatively coarse estimates for the quantities $\langle s\rangle$ and $\langle \tau j\rangle$ For $\langle \tau s\rangle$, however, a much better estimate is needed because this matrix element has a large weight.

Since the main interest in this paper is focussed on low-lying states, it is assumed that for the wave functions a pure j^n configuration may be taken. Then one obtains [5]

$$\langle s\rangle = \pm \frac{\langle j\rangle}{2l+1} = \pm \frac{J}{2l+1} \text{ for } j = l \pm \tfrac{1}{2}, \tag{3.4}$$

since within a pure j^n configuration $\vec{s}(i)$ is proportional to $\vec{j}(i)$, and

$$\langle \tau j\rangle = nT_3\left[6j(j+1)(2j+1)\frac{2T+1}{T(T+1)}\,\frac{J(2J+1)}{(J+1)}\right]^{\frac{1}{2}} *$$

$$* \sum_{\alpha_1 T_1 J_1} (-1)^{T_1+J_1+T+J+j+\frac{1}{2}} \begin{Bmatrix} \frac{1}{2} & T & T_1 \\ T & \frac{1}{2} & 1 \end{Bmatrix} \begin{Bmatrix} j & J & J_1 \\ J & j & 1 \end{Bmatrix} [j^{n-1}(\alpha_1 T_1 J_1) jTJ \,|\, \} j^n \alpha TJ]^2. \tag{3.5}$$

The summation is taken over all possible parent states $(\alpha_1 T_1 J_1)$. In the simple case of $J=j$, $T=\frac{1}{2}$, seniority $v=1$ and reduced isospin $t=\frac{1}{2}$, (3.5) can, for odd Z, be written as [5]

$$\langle \tau j\rangle = \begin{cases} j\left[1 - \dfrac{N_j}{3(j+1)}\right] & \text{for } Z = N+1 \\[2ex] -j\left[1 - \dfrac{2j+1-N_j}{3(j+1)}\right] & \text{for } Z = N+1 \end{cases},$$

where N_j denotes the number of neutrons in the j orbit. Since the operator $\sum_{i=1}^{A} \tau_3(i)\vec{j}(i)$ has no matrix elements connecting different j-j coupling configurations [5], small admixtures of other components to the wave function will change the matrix element $\langle \tau j \rangle$ only in second order and hence (3.5) is expected to give quite accurate estimates.

For the evaluation of $\langle \tau s \rangle$ use can be made of the experimental ft values for the β-decay between analogue states. The ft value is given by [9]

$$ft = \frac{B}{\langle 1 \rangle^2 + R^2 \langle \sigma \rangle^2}, \tag{3.6}$$

where B = 6170 ± 4 s [10] and R = 1.250 ± 0.009 [11]. The value for B stems from superallowed $0^+ \rightarrow 0^+$ β-decay in various nuclei with A = 10-54, but the coupling-constant ratio R is determined from free neutron decay and might be considerably quenched in nuclear matter [12]. The Fermi matrix element $\langle 1 \rangle$ differs from zero only for transitions connecting isobaric analogue states and then it is given by

$$\langle 1 \rangle^2 = T(T+1) - T_3^{initial} \times T_3^{final}. \tag{3.7}$$

The Gamow-Teller matrix element $\langle \sigma \rangle$ can be related to $\langle \tau s \rangle$ by (see also [9])

$$\langle \sigma \rangle^2 = 4 \frac{J+1}{J} \langle \tau s \rangle^2 \tag{3.8}$$

for β-transitions involving the analogue state of the nucleus with $|T_3| = T$. Thus the absolute value of $\langle \tau s \rangle$ can be computed from the experimental ft values of the β-decay between corresponding isobaric analogue states [3]. As has been pointed out [13], the mesonic corrections for β-decay and magnetic moments are somewhat different. In view of the inaccuracies introduced by the simplifying assumptions

that were made earlier these small effects will consequently be neglected. The fact that the left-hand equality of (3.4) also holds for $\langle\tau s\rangle$ and $\langle\tau j\rangle$ in a pure j^n configuration, can be used to extract a tentative sign of the former with the help of (3.5). This also enables us to express the isovector g-factor as a function of either of these two matrix elements

$$g_1 = \begin{cases} [-\tfrac{1}{2} \mp \frac{4.206}{21+1}]\ \frac{\langle\tau j\rangle}{J} & (3.9^a) \\ & \text{, for } j = l \pm \tfrac{1}{2}. \\ [\mp(21+1)-8.412]\frac{\langle\tau s\rangle}{2J} & (3.9^b) \end{cases}$$

Here the bare-nucleon spin and orbital g-factors have been inserted.

4. Comparison with experiment

Theoretical predictions concerning isoscalar g-factors g_0 can be compared directly with measured g-factors of selfconjugated nuclei (i.e. with $T_3 = 0$). For $T_3 \neq 0$ the magnetic moments of both isobaric analogue states have to be known and must be substituted in the left-hand equalities of (3.2) and (3.3) in order to extract g_0 and g_1. Table 2 summarizes the experimental information on isoscalar and isovector g-factors obtained from the compilation [6] and some recent references [14].

4.1. THE ISOSCALAR g-FACTOR

After insertion of free-nucleon values for spin and orbital g-factors in (3.2) one obtains with the help of (3.4)

$$g_0(j) = \tfrac{1}{2} \pm \frac{0.380}{21+1}\ , \qquad (4.1)$$

for $j = l \pm \frac{1}{2}$ in the description of a pure j^n configuration.

Table 2

Experimental values of the isoscalar g_o factors and the isovector g factors for mirror and selfconjugated nuclei [a,b)]

Nuclei, J^π ; T	g_o	g_1	Nuclei, J^π ; T	g_o	g_1
n/H , $1/2^+$; 1/2	0.880	-4.706	^{21}Ne/Na, $3/2^+$; 1/2	0.575	-1.016
^{2}H , 1^+ ; 0	0.857	--	^{21}Ne/Na, $5/2^+$; 1/2	0.59(5)	-0.89(5)
^{3}H/He , $1/2^+$; 1/2	0.851	+5.107	^{22}Na , 3^+ ; 0	0.582(1)	--
^{6}Li , 1^+ ; 0	0.822	--	^{22}Na , 1^+ ; 0	0.540(9)	--
^{8}Li/B , 2^+ , 1	0.672	+0.154	^{24}Mg , 2^+ ; 0	0.51(2)	--
^{10}B , 3^+ ; 0	0.600	--	^{25}Mg/Al, $5/2^+$; 1/2	0.558	-0.900
^{10}B , 1^+ ; 0	0.63(12)	--	^{26}Al , 3^+ ; 0	0.65(9)	--
^{11}B/C , $3/2^-$; 1/2	0.575	+1.218	^{29}Si/P , $1/2^+$; 1/2	0.680	-1.790
^{12}B/N , 1^+ ; 1	0.730	+0.273	^{31}P/S , $1/2^+$; 1/2	0.644	+1.620
^{13}C/N , $1/2^-$; 1/2	0.380	+1.025	^{32}S , 2^+ ; 0	0.47(9)	--
^{14}N , 1^+ ; 0	0.404	--	^{35}Cl/Ar, $3/2^+$; 1/2	0.485(1)	+0.063(1)
^{14}N , 2^- ; 0	0.62(5)	--	^{36}Cl/K , 2^+ ; 1	0.458(1)	+0.184(1)
^{15}N/O , $1/2^-$; 1/2	0.436(1)	-1.002(1)	^{37}Ar/K , $3/2^+$; 1/2	0.384(67)	+0.249(67)
^{16}O , 3^- ; 0	0.551(27)	--	^{37}Ar/K , $7/2^-$; 1/2	0.553(43)	-0.933(43)
^{17}O/F , $5/2^+$; 1/2	0.566	-1.323	^{38}K , 3^+ ; 0	0.458	--
^{18}F , 5^+ ; 0	0.572(6)	--	^{38}K , 7^+ ; 0	0.548(2)	--
^{18}F , 3^+ ; 0	0.58(7)	--	^{39}K/Ca , $3/2^+$; 1/2	0.471	-0.210
^{19}F/Ne, $1/2^+$; 1/2	0.742(1)	+4.516(1)	^{40}Ca , 5^- ; 0	0.54(10)	--
^{19}F/Ne, $5/2^+$; 1/2	0.573(2)	+0.869(2)	^{40}Ca , 3^- ; 0	0.56(13)	--
^{20}F/Na, 2^+ ; 1	0.616	+0.431	^{41}Ca/Sc, $7/2^-$; 1/2	0.548(3)	-1.004(3)
^{20}Ne , 2^+ ; 0	0.54(4)	--			

a) Errors smaller than the last digit are not given.

b) The experimental values stem from [6, 14].

In the low-mass region $A \lesssim 10$ wave functions in the LS-coupling scheme are expected to yield better results than in the j-j coupling scheme [15]. This changes neither the estimates for the $1s_{1/2}^n$ states obtained with (4.1) nor those for the $1p_{3/2}^n$ states as far as the odd-A nuclei are concerned. For the low-lying $1p_{3/2}^n$ states in odd-odd nuclei, however, one should use (3.2) with $\langle s \rangle = 1$ since in the LS scheme this is energetically more favourable than $\langle s \rangle = 0$.

A somewhat different approach is required when particles in different orbits are involved as in $^{12}B/N(1^+)$, $^{14}N(2^-)$, $^{16}O(3^-)$, $^{32}S(2^+)$ and $^{40}Ca(5^-,3^-)$. In such cases the additivity relation (2.1) must be applied to the values $g_o(j_i)$ $(i = 1,2)$ for each of the two orbits to obtain $g_o(j_1 \otimes j_2 = J)$. Then one also obtains the centre-of-gravity sum rule (for $j_1 > j_2$)

$$\frac{1}{2j_2+1} \sum_{J=j_1-j_2}^{j_1+j_2} g_o(j_1 \otimes j_2 = J) = g_o(j_1). \tag{4.2}$$

In fig. 1 the experimental values of g_o from table 1 are compared with the predictions of (4.1) (solid bars), the additivity estimates (triangles) and the LS-coupling results (+). The discrepancy for the mirror pair $^{19}F/Ne(1/2^+)$ [point marked (a) in fig. 1] has to be explained by a large $2s_{1/2}$ admixture. Indeed the average of the $1d_{5/2}$ and $2s_{1/2}$ estimates lies within 2% of the experimental value. The values for A = 37 and 38 [marked (b)] both refer to $1f_{7/2}^n$ excited states and should, as they do, correspond to the $1f_{7/2}$ estimate. A possible discrepancy for the second excited state of $^{26}Al(3^+)$ is removed by taking the $1d_{5/2}2s_{1/2}$ additivity result. The $2s_{1/2}$ estimates clearly show to be too high, owing to configuration mixing.

For all 41 experimental data and the values calculated with (4.1) and the additivity relation, one finds a mean absolute deviation of $\overline{|\delta g_o|} = 0.035$ and a root-mean-square deviation of $\sqrt{\overline{\delta g_o^2}} = 0.060$.

These numbers, however, are largely influenced by the poor agreement for A=29 and A=31. Omission of these two data yields $\overline{|\delta g_o|} =$

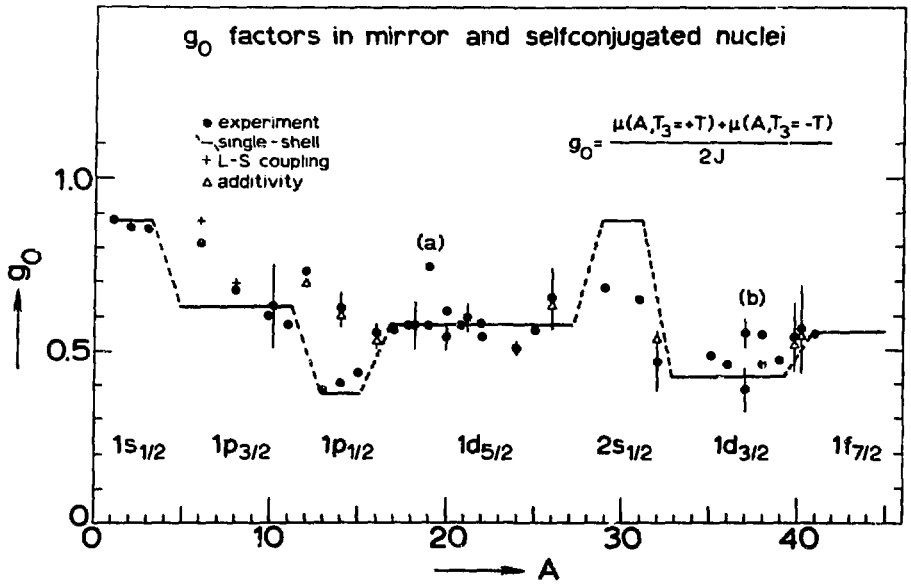

Fig. 1. A comparison between theory and experiment for g_o factors in mirror and selfconjugated nuclei. The points marked (a) and (b) are discussed in subsect. 4.1.

0.025 and $\sqrt{\overline{\delta g_o^2}}$ = 0.032 which is fully compatible with the results of recent large-scale shell-model calculations [16] $\overline{|\delta g_o|}$ = 0.020 and $\sqrt{\overline{\delta g_o^2}}$ = 0.030.

An insignificant improvement of the agreement is found with $(g_n^l+g_p^l)$ = 1.02 and $(g_n^s+g_p^s)$ = 1.64 inserted in (3.2), obtained in a least-squares fit to the data excluding the two $2s_{1/2}$ points. It has been argued [13] that the form of the magnetic-moment operator (3.2) has to be changed effectively by inclusion of a tensor term $\sum_{i=1}^{A} [Y^2(\theta_i,\phi_i).\vec{s}(i)]^{(1)}$. This leads to addition of a term proportional to $\pm\{1\mp\frac{j-l+1}{j+l}\}$, for j = $l\pm1/2$, in the pure j^n configuration estimates of (4.1). No improvement was found, however, upon inclusion of such a term or by considering a possible contribution from a two-body $\vec{L}.\vec{S}$ force ($\delta g_o \sim \pm\frac{1}{J}\cdot\frac{2j+1}{2j+2}$ [7]).

Finally the hypothesis of a pure j^n configuration was examined by comparing the values of <s> obtained from (3.4) with those deduced from experiment by means of the right-hand equality in (3.2)

and the free-nucleon spin and orbital g-factors. Though the signs of these matrix elements are correctly predicted, in about one third of the cases the experimental values of <s> deviate more than 25% from those calculated with (3.4). The theoretical values are too large in absolute magnitude except for the two $|T_3| = 1$ mirror pairs ^{12}B/N and ^{20}F/Na. No different behaviour of <s> is observed for those mirror pairs which have one particle or one hole with respect to an LS-closed core (^{15}N/O, ^{17}O/F, ^{39}K/Ca, ^{41}Ca/Sc). This could be expected since for these nuclei the mesonic exchange current contributes to g_1 only and as for these nuclei no first-order core-polarization effect exists, corrections to <s> had to be explained by second-order contributions [13].

4.2. THE ISOVECTOR g-FACTOR

Accurate experimental ft values, deduced from various half-life and branching-ratio measurements, of $T_3 = \frac{1}{2}$ nuclei are obtained from [17]. The agreement of the isovector g-factor values, calculated from these ft values through (3.3) with (3.5 - 3.8) and bare-nucleon g-factors, with the experimental values turned out to be rather poor. Excluding the mirror pair ^{19}F/Ne($1/2^+$), because of the uncertainty in the simple wave function, a mean absolute deviation of $\overline{|\delta g_1|} = 0.19$ and a root-mean-squared deviation of $\sqrt{\overline{\delta g_1^2}} = 0.23$ are found.

As has been stated previously, however, the ratio R of the coupling constants for Fermi and Gamow-Teller transitions may be quenched in multinucleon systems. In order to see how this could affect the results, R was treated as a free parameter in a fit to the data. A highly significant improvement emerged with R = 1.1 since then $\overline{|\delta g_1|} = 0.065$ and $\sqrt{\overline{\delta g_1^2}} = 0.093$. The results are given in table 3a. It is seen that also the average of the estimates for A=19, with either $|1d^3_{5/2} v=3, t=\frac{1}{2}, J=\frac{1}{2}\rangle$ or $|(1d^2_{5/2})_0 2s_{1/2}\rangle$ taken as the simple wave function, lies within 4% of the experimental value. It should be stressed that it may not be concluded that the 12% decrease in R resulting from the fit is realistic, since an identical improvement would also be found if the value of $(g^s_n - g^s_p)$ is increased by 10%. No evidence to support a change in the value of $(g^1_n - g^1_p)$ can be obtained from the procedure followed here.

Table 3a

The matrix elements $\langle\tau s\rangle$ and isovector g-factors as deduced from β-decay ft-values of $|T_3| = 1/2$ nuclei

A, J^π	ft [a)]	$\langle\tau s\rangle$ [b)]	$\langle s\rangle$ [c)]	g_1(theory)[d)]	g_1(exp)
3; $1/2^+$	1140(10)	-0.551(3)	+0.463	+5.137(25)	+5.107
11; $3/2^-$	3970(20)	-0.262(2)	+0.295	+1.235(5)	+1.218
13; $1/2^-$	4670(20)	-0.149(1)	-0.158	+0.751(11)	+1.025
15; $1/2^-$	4400(20)	+0.166(1)	-0.085(1)	-0.900(11)	-1.002(1)
17; $5/2^+$	2290(10)	+0.500(2)	+0.433	+1.341(3)	-1.323
19; $1/2^+$	1725(10)	-0.421(2)	+0.319(1)	+4.710(14)	+4.516
21; $3/2^+$	4050(30)	+0.255(3)	+0.296	-0.961(8)	-1.016
25; $5/2^+$	3730(20)	+0.311(2)	+0.381	-0.832(4)	-0.900
29; $1/2^+$	4770(50)	+0.142(3)	+0.237	-1.696(28)	-1.790
31; $1/2^+$	5015(60)	-0.126(4)	+0.189	+1.559(34)	+1.620
35; $3/2^+$	5705(20)	+0.101(2)	-0.059(3)	+0.085(6)	+0.063(1)
37; $3/2^+$	4585(35)	-0.207(3)	-0.458(264)	+0.214(9)	+0.249(67)
39; $3/2^+$	4290(25)	+0.233(2)	+0.114	-0.154(6)	-0.210
41; $7/2^-$	2860(20)	+0.431(3)	+0.442(28)	-1.018(4)	-1.004(3)

a) ft Values from [17] in s.

b) Deduced from ft values through (3.6-8) with R = 1.1. Sign assignment for the nucleus with odd Z as discussed in sect. 3.

c) Obtained from experimental g_o factors as discussed in subsect. (4.1).

d) Calculated with bare-nucleon spin and orbital g-factors. In all cases with J=j seniority v=1 is assumed in the evaluation of $\langle\tau j\rangle$; for A=19 the matrix element $\langle\tau j\rangle$ has been taken as the average over the $|(1d^3_{5/2})v=3,t=1/2,J=1/2\rangle$ and $|(1d^2_{5/2})_o 2s_{1/2}\rangle$ estimates of (3.5) and for A = 21 the $|1d^5_{5/2}$ v=5, t=1/2, J=3/2> estimate has been used.

Table 3b

g-Factors of $T_3 = +1/2$ nuclei compared with values calculated under the assumption of pure j^n configuration from ft values [a)]

Nucleus; J^π	ft	$\langle\tau s\rangle$	g_{calc} [b)]	g_{exp} [c)]
^{7}Li ; $3/2^-$	2300(100)	-0.457(16)	+2.274(44)	+2.171
^{23}Na; $3/2^+$	4705(20)	-0.196(2)	+1.482(5)	+1.478
^{27}Al; $5/2^+$	4125(10)	-0.270(1)	+1.531(2)	+1.457
^{33}S ; $3/2^+$	5560(70)	-0.117(7)	+0.251(21)	+0.429
^{43}Sc; $7/2^-$	3090(140)	-0.400(18)	+1.313(22)	+1.320(11)
^{51}Mn; $5/2^-$	3765(175)	-0.307(18)	+1.348(30)	+1.427(1)
^{55}Co; $7/2^-$	3725(105)	-0.325(11)	+1.444(12)	+1.378

a) ft-values from [17] in s; coupling constant ratio R = 1.1.

b) $g = g_o + g_1$, where g_o is calculated from (4.1) and g_1 from (3.3) as in table 3a. For ^{23}Na the $|1d^7_{5/2}$, v=3,t=1/2,J=3/2> and for ^{51}Mn the $|1f^{-5}_{7/2}$ v=3,t=1/2, J=5/2> estimate of (3.5) for $\langle\tau j\rangle$ have been taken.

c) From [6]; errors smaller than the last digit are not given.

For a number of isobaric T = 1/2 doublets only the magnetic moment of the neutron-rich, $T_3 = +1/2$, nucleus has been measured. These can be used to test simultaneously the reliability of the simple estimates from (4.1) for g_o and those from the ft values for g_1. The results are presented in table 3b. A mean absolute deviation of $\overline{|\delta g|} = 0.072$ and a root-mean-squared deviation of $\sqrt{\overline{\delta g^2}} = 0.090$ are found for the whole g-factor, in accordance with the results for g_o and g_1 separately.

The $|T_z| = 1$ isobaric doublets cannot be included in the present analysis owing to the large experimental inaccuracies in the ft values. Reversing the procedure outlined above to extract ft values from the experimental g_1- or g-factors shows an agreement to within the experimental errors. The latter are too large, however, to distinguish between R = 1.25 and R = 1.1.

Finally we will discuss some results that follow from the analysis of the matrix elements $\langle \tau s \rangle$ obtained from the ft values through (3.6 - 8). These are shown in table 3a together with the values of $\langle s \rangle$ obtained from the experimental g_o factors as discussed at the end of subsect. 4.1. It is observed that the two matrix elements $\langle \tau s \rangle$ and $\langle s \rangle$ are rather close in absolute magnitude and show a similar variation with A and J (see also [18]). By adding or subtracting these two, one obtains the matrix elements for the total spin of the proton group, $\langle (1-\tau_3).s/2 \rangle$, or the neutron group. It shows that the spins of the even group of identical nucleons couple almost to total spin zero, presumably because of the pairing effect. One finds that $\langle \sum_{\text{even group}} s \rangle$ in all cases is smaller than 0.07 and on the average is equal to 0.03. These results hold regardless whether the bare nucleon or the effective spin and orbital g-factors and coupling-constant ratio are used. Under the assumption that the same coupling to total spin zero takes place for both the proton and the neutron group in doubly-even nuclei, we can estimate the isoscalar g-factor of such nuclei from (3.2) as

$$g_o(\text{doubly-even}) = 0.50 + \Delta g_o, \text{ with } |\Delta g_o| \leq \frac{0.05}{J}. \tag{4.3}$$

Equation (4.3) generates highly accurate estimates for low-lying states in even-even nuclei, which are not inconsistent with the existing experimental data. A study of large shell-model values [16] for $\langle s \rangle$ of various states in doubly-even nuclei reveals a slight J-dependence of this matrix element. This results in a slightly weaker upper limit for Δg_o in (4.3) of $|\Delta g_o| \leq 0.05$.

As can be inferred from tables 3a and 3b the matrix elements $\langle \tau s \rangle$ generally are somewhat smaller in absolute value than the simple pure j^n prediction $\pm\langle \tau j \rangle/(2l+1)$, for $j = l \pm 1/2$, though their sign is obviously predicted correctly. From (3.5) it follows that mostly $|\langle \tau j \rangle| < J$. We can combine the above results on $\langle \tau s \rangle$ and $\langle \tau j \rangle$ to get a better understanding of the behaviour of g_l. For example, it follows from (3.9a) that for the $1d_{3/2}$ subshell $|g_l| < 0.35$. Furthermore for doubly-even nuclei one has $|\langle \tau s \rangle| \lesssim 0.13$, if the generalization from odd-even to even-even nuclei holds. It can be shown from (3.9a) and (3.5) that $|g_l| \lesssim 1$, where the maximum is reached for nuclei that consist of a jj-closed core plus or minus two identical nucleons. It follows from (3.3) and (3.9a,b) that for the other even-even nuclei generally one has $|g_l| \approx 0.1 - 0.4$. Though all the above rules or limits are not strict and moreover hold only for pure j^n configurations, they are obeyed by all g-factors measured so far.

5. Conclusions

The results of the previous sections can be summarized as follows.

(i) The additivity relation correlates experimental g-factors very well. Semi-empirical estimates of g-factors can be made with an uncertainty of about $\delta g \approx 0.01$. Perhaps the most important conclusion is that there seem to be no nonvanishing renormalizations of the g-factor that show a steeper than linear dependence on the number of valence protons and neutrons.

(ii) The behaviour of the isoscalar g-factor, g_o, is well understood when simple configurations are assumed. More sophisticated

multishell approaches do not improve the agreement significantly. There seems to be no need for additional renormalizations of the g-factor as far as g_o is concerned. The observed agreement for the isoscalar g-factors can be used to obtain half-experimental estimates with an uncertainty of $\delta g \approx 0.03$ for neutron-deficient nuclei from the known g-factors in analogue states of the neutron-rich member in the isobaric multiplet.

(iii) The relation between Gamow-Teller matrix-elements deduced from β-decay ft values and isovector g-factors holds well if the coupling constant ratio R is taken to be R = 1.1. This agrees with theoretical predictions of the quenching of this ratio in nuclear matter.

(iv) Finally a study of the matrix elements $\langle \tau s \rangle$, obtained from β-decay ft values, and $\langle s \rangle$, deduced from g_o factors, reveals that the even group of nucleons in an odd-A T = 1/2 nucleus has a total spin close to zero. By generalizing this notion to even-even nuclei the isoscalar part of their g-factors can be estimated with high precision. Also the behaviour of the trend for the isovector part can be understood qualitatively.

References

[1] I. Talmi, Phys. Rev. 83 (1951) 1248;
H.M. Schwarz, Phys. Rev. 89 (1953) 1293

[2] J.F.A. Van Hienen and P.W.M. Glaudemans, Phys. Lett. 42B (1972) 301

[3] K. Sugimoto, Phys. Rev. 182 (1969) 1051 and J.Phys. Soc. Jap. 34 Suppl. (1973) 197

[4] P.C. Zalm, A. Holthuizen, J.A.G. De Raedt and G. Van Middelkoop, Phys. Lett. 69B (1977) 157

[5] A. De-Shalit and I. Talmi, Nuclear Shell Theory (Academic Press, New York, 1963)

[6] V.S. Shirley and C.M. Lederer, in: Hyperfine Interactions (ed. E. Karlsson and R. Wäppling, Almqvist & Wiksell, Stockholm, 1975)

[7] M. Chemtomb, Nucl. Phys. A123 (1969) 449;
S. Wahlborn and J. Blomqvist, Nucl. Phys. A133 (1969) 50

[8] A. Arima and H. Horie, Progr. Theor. Phys. 12 (1954) 623

[9] M.G. Mayer and J.H.D. Jensen, Elementary Theory of Nuclear Shell Structure (Wiley, New York, 1955)

[10] I.S. Towner, J.C. Hardy and M. Harvey, Nucl. Phys. A284 (1977) 269

[11] A. Kropf and H. Paul, Z. Phys. 267 (1974) 129
[12] R.J. Blin-Stoyle, Nucl. Phys. A254 (1975) 353
[13] K. Shimizu, M. Ichimura and A. Arima, Nucl. Phys. A226 (1974) 282
[14] R.E. Horstman, J.L. Eberhardt, H.A. Doubt, C.M.E. Otten and G. Van Middelkoop, Nucl. Phys. A248 (1975) 291;
T. Minamisono, J.W. Hugg, D.G. Mavis, T.K. Saylor, H.F. Glavish and S.S. Hanna, Phys. Lett. 61B (1976) 155;
T. Minamisono, J.W. Hugg, J.R. Hall, D.G. Mavis, H.F. Glavish and S.S. Hanna, Phys. Rev. C14 (1976) 376;
T. Minamisono, J.W. Hugg, J.R. Hall, D.G. Mavis, D.L. Clark and S.S. Hanna, Phys. Rev. C14 (1976) 2335;
H.C. Jain, A. Little, S.M. Lazarus, T.K. Saylor, B.B. Triplett and S.S. Hanna, Phys. Rev. C14 (1976) 2013;
M. Akiba, T. Hattori and K. Misatake, J. Phys. Soc. Jap. 40 (1976) 307;
Various results reported at : Hyperfine Interactions IV (Madison, 1977)
[15] S. Varma and P. Goldhammer, Nucl. Phys. A125 (1969) 193
[16] F. Meurders, P.W.M. Glaudemans, J.F.A. Van Hienen and G.A. Timmer, Z. Phys. A276 (1976) 113;
F.E.H. Van Eijkern, G.A. Timmer and P.W.M. Glaudemans, Z. Phys. A278 (1976) 337;
W. Chung and B.H. Wildenthal, to be published
[17] I. Tanihata, T. Minamisono, A. Mizobuchi and K. Sugimoto, J. Phys. Soc. Jap. 34 (1973) 848;
G. Azuelos and J.E. Kitching, Phys. Rev. C12 (1975) 563;
G. Azuelos, J.E. Kitching and K. Ramavataram, Phys. Rev. C15 (1977) 1847
[18] R. Leonardi and M. Rosa-Clot, Phys. Rev. Lett. 24 (1970) 407.

CHAPTER II

SIMPLE RELATIONS FOR NUCLEAR MOMENTS (II)
(electric quadrupole moments of quasi-rotational states in even-even nuclei)

1. Introduction

In this chapter a simple expression is derived which relates the electric quadrupole moments of quasi-rotational states of even-even nuclei to the excitation energies of the corresponding levels. As a starting point in the description of nuclear collective phenomena the rotationally invariant core (RIC) model [1] is chosen, which is a special case of the two-fluid model.

It will be shown that for a broad class of ellipsoidal shaped density distribution functions the requirement of volume conservation in the RIC model results to first order in a linear relationship between the electric quadrupole moment and the moment of inertia. Only the second-order term depends on the particular choice of the distribution.

In the next step the moment of inertia is expressed as a function of the excitation energy. A test of the proposed relation is provided by a comparison of 95 experimental values of static electric quadrupole moments of even-even nuclei and those calculated from the excitation energies on the basis of the derived expressions.

Finally the relation will be compared with other simple approaches that were applied to transitional quadrupole moments deduced from intraband electric quadrupole transitions. Implications of the observed agreement will be discussed.

2. Derivation of the relations

2.1. THE MODEL

Let us consider an even-even nucleus of mass A, which is supposed to show an axially symmetric state-dependent deformation. The charge and mass density distributions are assumed to be identical. In the RIC model a deformed nucleus is considered to consist of two parts, a spherical superfluid core that does not participate in the collective motion plus a normal outer fluid that rotates bodily about it with a rigid-body moment of inertia [1]. In this model the superfluid core is assumed to occupy the largest spherical volume that can be accommodated within the deformed nucleus. A rather schematic graphical representation of the RIC model is given in fig. 1.

For the derivation of the relations presented in this chapter, we will restrict ourselves to the broad class of ellipsoidal density distributions $f(\xi)$. Here f is a monotonic one-parameter function with nonvanishing and finite second and fourth moments. The parameter ξ is related to the intrinsic coordinates $\vec{r} = (x, y, z)$ in the body-fixed frame by

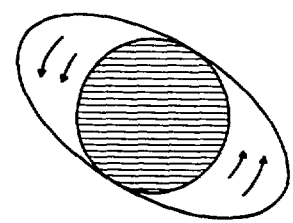

Fig. 1. A schematic representation of the RIC model.

$$\xi^2 = \frac{x^2 + y^2}{a^2(\varepsilon)} + \frac{z^2}{b^2(\varepsilon)} , \tag{2.1}$$

where ε represents a deformation parameter. Clearly the z-axis is the symmetry axis of the nucleus. For vanishing deformation the distribution must be spherical, i.e. $a(0) = b(0)$. The total volume of the deformed nucleus, $V(\varepsilon)$, is taken to be constant to first order in ε, i.e.

$$V(\varepsilon) = \frac{4\pi}{3} R_o^3 \, [1 + \mathcal{O}(\varepsilon^2)], \tag{2.2}$$

where as usual the nuclear radius is given by $R_o = 1.2\ A^{1/3}$ fm. From (2.1) and (2.2) it follows that one may write

$$a(\varepsilon) = R_o\ [1 - \varepsilon/2 + \mathcal{O}(\varepsilon^2)],$$
$$b(\varepsilon) = R_o\ [1 + \varepsilon + \mathcal{O}(\varepsilon^2)], \tag{2.3}$$

irrespective of the precise functional form of f. Hence for $\varepsilon > 0$ we have a so called prolate (cigar-shaped) deformation and for $\varepsilon < 0$ an oblate (disk-shaped) deformation. For simplicity we shall assume that there is no term proportional to ε^2 in (2.3), but this is not essential for the derivation.

An important consequence of the class of functions that has been chosen is that the density distribution of the superfluid core, the largest spherical density that can be accommodated within the density distribution $f(\xi)$ of the deformed nucleus, is given by $f(\xi^*)$, where ξ^* satisfies the condition

$$\xi^* = r/\min\ [a(\varepsilon),\ b(\varepsilon)]. \tag{2.4}$$

Two especially interesting shapes of density distributions of the above type are the uniform distribution, $f(\xi) = 1$ if $\xi^2 \leq 1$ and $f(\xi) = 0$ otherwise, and the Gaussian distribution, $f(\xi) = \exp[-\xi^2/2]$. For the uniform distribution it is necessary to assume a sharp, frictionless, slippage surface between the superfluid core or radius ξ^* and the outer fluid; this assumption, however, is not very realistic. For this reason the RIC model has been subject to criticism [2], but the argument certainly does not hold for the more realistic, gaussian density distribution, where the active particles, or nuclear matter, participating in the collective motion penetrate the core. In such a case the RIC model manifests itself as the true "collective analogue" of the microscopic shell model.

2.2 EXPLICIT EXPRESSIONS

With a density distribution of the type discussed in the previous subsection, the intrinsic quadrupole moment Q_o for a nucleus

with charge eZ is readily evaluated to be

$$Q_o = eZ\langle 3z^2-r^2\rangle = 2eZ\langle z^2-x^2\rangle = 2\eta eZR_o^2\varepsilon(1+\frac{\varepsilon}{4}), \tag{2.5}$$

where the average has been taken over the intrinsic coordinates. The geometrical constant η is given by $\eta = \int_o^\infty \xi^4 f(\xi)d\xi \Big/ \int_o^\infty \xi^2 f(\xi)d\xi$ and is independent of ε. E.g. for a uniform and a gaussian density distribution one finds $\eta = 3/5$ and $\eta = 3$, respectively.

The rigid-body moment of inertia $\mathcal{J}$ of the rotating outer fluid is conveniently computed by evaluating the difference between the rigid-body moments of inertia of the whole deformed density distribution, $f(\xi)$, and the spherical distribution of the superfluid core, $f(\xi^*)$. Thus, for the y-axis as the axis of rotation, one may write

$$\mathcal{J} = mA\langle x^2+z^2\rangle - mA^*\langle x^2+z^2\rangle^*, \tag{2.6}$$

where m is the single-nucleon mass and the asterisk indicates that the average is taken over the spherical core. From the formulation of the RIC model it follows that $A^* = A \min(a/b, [b/a]^2)$ and $\langle x^2+z^2\rangle^* = 2 \min(\langle x^2\rangle, \langle z^2\rangle)$ depend on the sign of the deformation parameter ε. Hence (2.6), in combination with (2.5), leads directly to the relation

$$\mathcal{J} = \frac{mA}{eZ} Q_o \begin{cases} 1+\mathcal{O}\left[\dfrac{Q_o}{eZ\eta R_o^2}\right], & \text{for } \varepsilon > 0, \\[2ex] -\dfrac{3}{2}+\mathcal{O}\left[\dfrac{Q_o}{eZ\eta R_o^2}\right], & \text{for } \varepsilon < 0 \end{cases} \tag{2.7}$$

Thus it shows that the notion of volume conservation leads in first order to a linear relation between $\mathcal{J}$ and Q_o. This linear relationship is independent of a particular form of the nuclear density distribution within the selected class of functions.

The intrinsic quadrupole moment Q_o of the rotational state with angular momentum I that belongs to the K-band is related to the spectroscopic quadrupole moment Q_s by [3]

$$Q_s = Q_o \frac{3K^2 - I(I+1)}{(I+1)\,(2I+3)} \,. \tag{2.8}$$

The moment of inertia $\mathcal{J}$ of such a state can be obtained from the excitation energy if the relation for rotational spectra [3]

$$E_{K,I} = E_K^o + \frac{\hbar^2}{2} \frac{I(I+1) - K^2}{\mathcal{J}} \tag{2.9}$$

is assumed to apply. That is, the moment of inertia is considered to be state dependent and its behaviour is taken to be well described in the RIC model.

By the use of (2.7) - (2.9) an expression for the spectroscopic electric quadrupole moment of a rotational state in an even-even nucleus in terms of the excitation energy is obtained,

$$Q_s = \frac{3K^2 - I(I+1)}{(I+1)\,(2I+3)}\, 21.0\, \frac{Z}{A}\, \Theta \begin{cases} 1 + \dfrac{8.2}{\eta} \dfrac{\Theta}{A^{5/3}}\,, & \text{for } \varepsilon > 0, \\[2ex] -\dfrac{2}{3} - \dfrac{6.5}{\eta} \dfrac{\Theta}{A^{5/3}}\,, & \text{for } \varepsilon < 0. \end{cases} \tag{2.10}$$

Here we have introduced for convenience $\Theta = 2\mathcal{J}/\hbar^2$. In (2.10) the constants have been inserted such that Q_s is given in units of $[ef^2m]$ if Θ is given in $[MeV^{-1}]$. As can be seen, the details of the dependence on the distribution are contained in the second-order term of (2.10) as the geometrical constant η.

Before we turn to a comparison with experiment it may be worthwhile to mention that (2.10) holds for an even larger variety of

density distribution functions than the special class under consideration. For example, for the most widely used type of deformation in the study of nuclear collective motion, i.e. the quadrupole deformation [3], $f(r,\theta)=1$ for $r(\theta)\leq R_o[1+\beta_2 Y_{20}(\theta)] = R_o(1-\frac{\varepsilon}{2}+\frac{3\varepsilon}{2}\cos^2\theta)$ and $f(r,\theta)=0$ otherwise, we also find the relation (2.10) but with $\eta \approx 1.05$.

3. Comparison with experiment

3.1. DATA SELECTION

Most of the experimentally available values of static electric quadrupole moments of even-even nuclei refer to $I^\pi = 2^+$ states that belong to the K=0 ground-state band. They have been measured almost exclusively with the Coulomb excitation reorientation technique (CER), which involves a large number of higher-order effects [4]. As a consequence the results of the older CER experiments are not always reliable as the knowledge of the possible corrections was still incomplete. A notorious example form the various CER measurements on the first excited 2^+ state of ^{114}Cd reported before 1970 (see e.g. [5]). Recent experiments, however, show a good consistency as can be seen, for example, from a series of independent measurements on even Te isotopes quoted in [6]. In view of this the following acceptance policy for CER data was adopted: (i) All data published after the 1972 Osaka conference on nuclear moments, where the experimental techniques and methods of analysis were carefully scrutinized, were used. (ii) If for a certain level no recent data were available only the latest results from the period 1970-1971 were taken and in no case older data were accepted. This selection resulted in a negligible reduction but a considerably higher reliability and consistency of the adopted data set.

Another problem with the CER experiments concerns the sometimes unknown sign of the interference term that results from products of matrix elements that involve higher excited states [4]. In such cases, mainly in the mass region $A \approx 75-135$, generally two values result from experiment, corresponding to either sign of the inter-

ference term. Experiment shows [7] that for ^{102}Ru and ^{104}Ru as well as for ^{108}Pd and ^{110}Pd the interference is constructive, in accordance with the theoretical vibrational limit [8]. On the basis of this experimental evidence constructive interference was assumed for all quadrupole moments in the region Z = 32-52.

The experimental values of static quadrupole moments of even-even nuclei from a compilation [9] and recent references [6,7,10], that meet the above criteria, are summarized in table 1.

3.2. RESULTS

For a comparison between experimental values of static quadrupole moments and the theoretical predictions that follow from (2.10) the geometrical constant η was taken to be unity. This seems to be a reasonable initial value since $\eta=1$ yields predictions inbetween the estimates for a gaussian ($\eta=3$) and a uniform ($\eta=\frac{3}{5}$) distribution and since it is also close to the results for a quadrupole deformation. Another problem forms the sign of the deformation parameter ε which governs the sign of the quadrupole moments. This sign was simply taken to agree with experiment.

The quantity $\Theta = 2\mathcal{J}/\hbar^2$ was computed from (2.9) with the excitation energies and band assignments of [11]. For the K=0 ground-state band it satisfies the relation $\Theta = I(I+1)/E_I$ [MeV^{-1}]. For the two second-excited 2^+ states in ^{166}Er and ^{186}W that belong to the K=2 band, Θ was estimated under the assumption of a constant moment of inertia $\mathcal{J}$.

The results for the static quadrupole moments are given in table 1. In general the agreement is very good with a slight exception for the heavy Pd, the Cd, the light Te, the Nd and the Sm isotopes. For example all 37 nuclei up to and including the Ru isotopes show an overall goodness-of-fit of $\chi^2 = 1.0$. For the 22 nuclei ranging from Gd to Pb one finds $\chi^2 = 0.5$.

At this stage it is worthwhile to mention that no attempt has been made to pre-select the data with respect to the fact whether or not a certain nucleus appears to show a (quasi-)rotational spectrum. It may well be that typical vibrational nuclei, i.e. Pd, Cd, Te etc., and also transitional nuclei, like Nd and Sm, cannot be described in a simple rotational picture. For the light nuclei

Table 1

Comparison of experimental values for electric quadrupole moments of quasi-rotational states in even-even nuclei with those obtained from the excitation energy on the basis of the rotationally invariant core model

Nucleus; E_x a)	Q_{exp} b)	Q_{calc} c)	Nucleus; E_x a)	Q_{exp} b)	Q_{calc} c)
^{18}O ; 1.980	-10(3)	-10	^{74}Ge ; 0.596	-25(10)	-28
^{20}Ne ; 1.634	-21(4)	-13	^{76}Ge ; 0.563	-15(10)	-29
^{22}Ne ; 1.275	-15(3)	-16	^{76}Se ; 0.559	-31(4)	-31
^{24}Mg ; 1.369	-21(4)	-16	^{78}Se ; 0.614	-28(7)	-27
^{26}Mg ; 1.809	-14(5)	-10	^{80}Se ; 0.666	-32(6)	-24
^{28}Si ; 1.779	+14(4)	+ 8	^{82}Se ; 0.655	-22(7)	-24
^{32}S ; 2.230	- 7(2)	- 9	^{94}Mo ; 0.871	-13(8)	-19
^{34}S ; 2.127	+ 3(2)	+ 6	^{96}Mo ; 0.778	-20(8)	-21
^{36}Ar ; 1.970	+11(6)	+ 7	^{98}Mo ; 0.787	-20(9)	-20
^{40}Ar ; 1.461	+ 1(4)	+ 8	^{100}Mo ; 0.536	-35(6)	-29
^{42}Ca ; 1.524	-19(8)	-12	^{100}Ru ; 0.540	-40(12)	-29
^{44}Ca ; 1.157	-14(7)	-15	^{102}Ru ; 0.475	-34(8)	-34
^{46}Ti ; 0.889	-21(6)	-21	^{104}Ru ; 0.359	-76(19)	-45
^{48}Ti ; 0.983	-18(1)	-18	^{102}Pd ; 0.556	-20(15)	-29
^{50}Ti ; 1.555	+8(16)	+ 7	^{104}Pd ; 0.556	-28(12)	-30
^{50}Cr ; 0.783	-36(7)	-24	^{106}Pd ; 0.512	-56(8)	-32
^{52}Cr ; 1.434	-14(8)	-12	^{108}Pd ; 0.434	-53(5)	-37
^{54}Cr ; 0.835	-21(8)	-21	^{110}Pd ; 0.374	-59(7)	-42
^{56}Fe ; 0.847	-25(6)	-21	^{106}Cd ; 0.633	-24(7)	-27
^{58}Ni ; 1.454	-10(6)	-12	^{108}Cd ; 0.633	-42(7)	-26
^{60}Ni ; 1.333	- 9(4)	-13	^{110}Cd ; 0.658	-36(8)	-25
^{62}Ni ; 1.172	+5(12)	+10	^{112}Cd ; 0.617	-39(8)	-26
^{64}Zn ; 0.992	-14(2)	-18	^{114}Cd ; 0.558	-35(5)	-28
^{70}Zn ; 0.884	-21(3)	-18	^{116}Cd ; 0.514	-42(8)	-30

Table 1 (continued)

Nucleus;	E_x	Q_{exp}	Q_{calc}	Nucleus;	E_x	Q_{exp}	Q_{calc}
^{112}Sn ;	1.257	- 6(9)	- 13	^{154}Sm ;	0.082	-133(46)	-200
^{116}Sn ;	1.293	- 11(4)	- 12	^{156}Gd ;	0.089	-193(19)	-186
^{118}Sn ;	1.230	- 13(11)	- 13	^{158}Gd ;	0.080	-191(12)	-207
^{120}Sn ;	1.172	+ 2(7)	+ 9	^{160}Gd ;	0.075	-189(23)	-217
^{122}Sn ;	1.140	- 8(14)	- 13	^{160}Dy ;	0.087	-176(39)	-191
^{124}Sn ;	1.139	- 8(10)	- 13	^{164}Dy ;	0.073	-203(20)	-224
^{122}Te ;	0.564	- 44(6)	- 28	^{166}Er ;	0.081	-190(40)	-205
^{124}Te ;	0.602	- 45(5)	- 26	^{166}Er ;	0.265 †	-267(90)	-265
^{126}Te ;	0.666	- 23(5)	- 23	^{166}Er ;	0.786 *	+200(32)	+227
^{128}Te ;	0.743	- 22(5)	- 20	^{170}Er ;	0.079	-195(21)	-201
^{130}Te ;	0.840	- 12(5)	- 17	^{170}Yb ;	0.084	-212(36)	-195
^{130}Ba ;	0.357	- 33(24)	- 45	^{172}Yb ;	0.078	-216(37)	-209
^{134}Ba ;	0.605	- 33(13)	- 25	^{174}Yb ;	0.076	-212(25)	-211
^{136}Ba ;	0.818	- 19(17)	- 18	^{176}Yb ;	0.082	-222(38)	-199
^{138}Ba ;	1.436	- 7(15)	- 10	^{186}W ;	0.737 *	+130(30)	+124
^{140}Ce ;	2.083 †	- 39(8)	- 31	^{184}Os ;	0.120	-240(110)	-133
^{142}Ce ;	0.641	- 12(9)	- 23	^{186}Os ;	0.137	-147(54)	-114
^{144}Nd ;	0.696	- 39(21)	- 22	^{188}Os ;	0.155	-102(21)	- 99
^{146}Nd ;	0.454	- 72(20)	- 33	^{190}Os ;	0.187	- 99(19)	- 80
^{148}Nd ;	0.302	-136(30)	- 50	^{192}Os ;	0.206	- 62(21)	- 71
^{150}Nd ;	0.130	-200(51)	-121	^{194}Pt ;	0.328	+ 77(50)	+ 30
^{148}Sm ;	0.550	- 62(36)	- 28	^{204}Pb ;	0.889	+ 19(14)	+ 11
^{150}Sm ;	0.334	-125(20)	- 46	^{204}Pb ;	1.274 †	+ 30(20)	+ 33
^{152}Sm ;	0.122	-165(19)	-132				

a) All states are $(I^{\pi}, K) = (2^+, 0)$ except †, $(4^+, 0)$, and *, $(2^+, 2)$.
Band assignment and E_x [MeV] from [11].

b) Weighted averages from [6, 7, 9, 10]; Q in [efm^2].

c) Calculated from equation (2.10) with $\eta = 1$ and the sign adopted from experiment.

($A \lesssim 70$), however, which show neither a true rotational nor a vibrational spectrum the predictions of (2.10), based on the rotational model, generally are rather accurate. For typical rotational nuclei, like Yb, the agreement is very good as can be seen from table 1. Also it should be noted that the trend with mass number or excitation energy for a series of isotopes is well reproduced.

Finally the influence of the geometrical constant η upon the observed agreement was tested. It appeared that η could vary between 3/5, the uniform distribution value, and 3, the gaussian distribution value, without any significant influence on the quality of the agreement. This led to an attempt to renormalize the second-order term of (2.10) into the constant governing the magnitude of the first-order term. As a result the linear dependence on Z/A and Θ, i.e.

$$Q_s = \frac{3K^2 - I(I+1)}{(I+1)\,(2I+3)}\,\frac{Z}{A}\,\Theta_*(22.5 \pm 0.5)_* \begin{cases} 1 \text{ for } \varepsilon > 0 \\ -\frac{2}{3} \text{ for } \varepsilon < 0 \end{cases}, \tag{3.1}$$

was found to be compatible with (2.10).

4. Additional remarks and conclusion

4.1. OTHER SIMPLE ESTIMATES

Until recent years almost no reliable data for static quadrupole moments of even-even nuclei could be obtained directly from experiment. On the other hand B(E2) values for intraband electric quadrupole transitions can be related to the intrinsic quadrupole moment in the adiabatic rotor model to give [3]

$$B(E2,\ I_i \to I_f) = \frac{5}{16\pi}\,Q_o^2\,(2I_f+1)\begin{pmatrix} I_f & 2 & I_i \\ -K & 0 & K \end{pmatrix}^2, \text{ for } K \neq \tfrac{1}{2},\ 1, \tag{4.1}$$

In combination with (2.8) this leads e.g. for 2^+ states that belong to the K=0 ground-state band to $|Q_{02}| = 0.906\sqrt{B(E2,\ 0^+ \to 2^+)}$.

The main theoretical interest in simple relations between charge distributions of rotational even-even nuclei and excitation energies or moments of inertia has been focussed on these B(E2) values. It is by now well established [5], however, that values of static quadrupole moments deduced from B(E2) values through (4.1) often deviate considerably from those measured directly in e.g. CER experiments. This could be understood by noting that (4.1) is valid only when the states that belong to the same band have the same intrinsic state; i.e. they should all show the same moment of inertia, which is seldom true. For those nuclei where the spectra closely follow the I(I+1) law, e.g. for $E_{4+}/E_{2+} \gtrsim 3.2$ (theoretically 3.33) in the K=0 ground-state band, such as the Gd, Dy, Er and Yb isotopes listed in table 1 (see also [11]), the transition quadrupole moments Q_{02} generally come close to the static quadrupole moments. For the heavy actinides the I(I+1) rule holds extremely well ($E_{8+}/E_{2+} \gtrsim 11.3$; theoretically 12), thus one might expect (4.1) to yield transitional quadrupole moments close to the "true" static values which have not yet been measured. We shall compare the presently deduced formula (3.1) with other simple relations based on transitional quadrupole moments Q_{02}, obtained from B(E2, $0^+ \rightarrow 2^+$) measurements in this region [14].

In 1962, Grodzins [12] discovered an empirical, linear relationship between B(E2, $0^+ \rightarrow 2^+$) values for ground-band transitions and the quantity Z^2/AE_2. With accurate B(E2) values that are presently available this would lead to the relation

$$|Q_{02}| \approx 10.4\ Z/\sqrt{AE_2}\ [\mathrm{efm}^2] \tag{4.2}$$

with E_2 in MeV.

In 1969, Mariscotti et al.[13] proposed a variable moment of inertia (VMI) picture to explain the deviations of rotational spectra from the I(I+1) law. Their analogy for the energy equation (2.9) reads

$$E_I = \alpha(\mathcal{J}_o - \mathcal{J}_I)^2 + \frac{I(I+1)}{\mathcal{J}_I}\ , \tag{4.3}$$

with the auxiliary condition $\partial E/\partial \mathcal{J} = 0$. It was observed [13] that the transition quadrupole moment Q_{02} was in good approximation proportional to the square root of the transition moment of inertia $\mathcal{J}_{02}$ defined by $\mathcal{J}_{02} = (\mathcal{J}_0 + \mathcal{J}_2)/2$. For almost perfect rotors one has $\mathcal{J}_0 \approx \mathcal{J}_2$ and then the observed relation for the VMI model (ref.[13]) is in extremely good approximation given by

$$|Q_{02}| \approx 61.6/\sqrt{E_2}[\mathrm{efm}^2]. \tag{4.4}$$

For the heavy actinides $Z/\sqrt{A} \approx 6$ and hence (4.2) and (4.4) lead to results that agree to within 3%. In fig. 2 the transitional quadrupole moments Q_{02}, deduced from B(E2) values in this region [14], are compared with (i) the results from (3.1) with $\varepsilon > 0$, i.e. for a prolate deformation, and (ii) the results of (4.2) or the almost identical results of (4.4). The average is taken over the theoretical predictions for ^{238}U and ^{238}Pu and for ^{244}Pu and ^{244}Cm, since these are not very different and we are only interested in the trend in the data. As can be seen from fig. 2, the re-

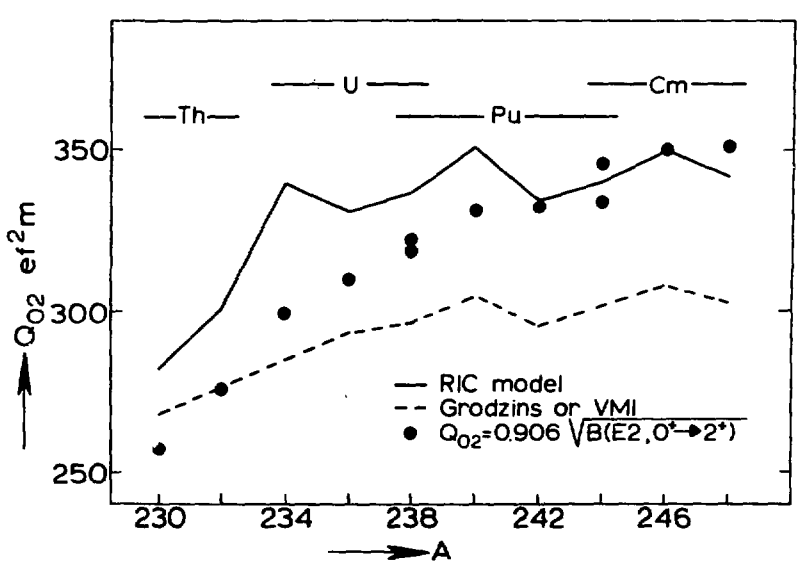

Fig. 2. A comparison between experimental values of transitional quadrupole moments for the heavy actinides and the trend predicted by the two simple approaches.

sults of (3.1) represent this trend slightly better than those from Grodzins formula or the VMI model, that were especially developed for transitional moments.

Finally it is worthwhile to mention an entirely different simple approach. It has been shown theoretically [15] that for energies of corresponding states (I^{π}, K) in even-even nuclei one has

$$E(Z, N) - E(Z, N+2) - E(Z+2, N) + E(Z+2, N+2) \approx 0, \qquad (4.5)$$

and that a similar relation holds for B(E2) values. In fact, (4.5) implies that the energy-dependence on Z and N can be written in a Taylor-series with small, or negligible, second- and higher-order terms. From (2.10), and also (3.1) and (4.2), it follows that if the energies of the states in even-even nuclei are a smooth function of Z and N, then also the B(E2) and Q values show a similar smooth trend. Thus one expects from (2.10) and (4.5) a relation like (4.5) to hold for quadrupole moments. Indeed, within the experimental errors, the available data in table 1 support the relation

$$Q(Z, N) - Q(Z, N+2) - Q(Z+2, N) + Q(Z+2, N+2) \approx 0,$$

for even-even nuclei.

4.2. CONCLUSION

In this chapter it has been shown that under fairly general conditions a simple expression can be derived for the RIC model, which relates static electric quadrupole moments and excitation energies of quasi-rotational states in even-even nuclei. This relation is shown to be only weakly dependent on the detailed structure of the nucleon density distribution.

The observed agreement with experiment supports the basic idea underlying the RIC model. That is, it suggests that nuclei rotate bodily instead of irrotationally, but only a fraction of the nucleus participates in the rotational motion.

A restriction in the use of the relation is that the shape of

the nucleus has to be known. Theory can solve this problem by the study of shape transitions in series of isotopes (see e.g. [16]). As far as large quadrupole moments are concerned, theory may provide simple sign attributions based on subshell-sequences in neighbouring nuclei [17]. Experimentally, it has been shown [18] that α-γ angular correlations can be highly sensitive to the sign of the quadrupole moment.

References

[1] L.E.H. Trainor and R.K. Gupta, Can. J. Phys. 49 (1971) 133
[2] R.A. Sorensen, Rev. Mod. Phys. 45 (1973) 353
[3] D.J. Rowe, Nuclear Collective Motion (Methuen & Co Ltd., London, 1970)
[4] O. Häusser, in: Nuclear Spectroscopy and Reactions, C (ed. J. Cherny, Academic Press, New York, 1974)
[5] A. Christy and O. Häusser, Nuclear Data A11 (1972) 281
[6] A. Bockisch and A.M. Kleinfeld, Nucl. Phys. A261 (1976) 498
[7] C. Fahlander, L. Hasselgren, J.E. Thun, A. Bockisch, A.M. Kleinfeld, A. Gelberg and K.P. Lieb, Phys. Lett. 60B (1976) 347;
L. Hasselgren, C. Fahlander, F. Falk, L.O. Edvardson, J.E. Thun, B.S. Ghuman and B. Skaali, Nucl. Phys. A264 (1976) 341;
C. Fahlander, Ph.D. Thesis, Uppsala 1977
[8] K. Kumar, Phys. Lett. 29B (1969) 25
[9] V.S. Shirley and C.M. Lederer, in: Hyperfine Interactions (ed. E. Karlsson and R. Wäppling, Almqvist & Wiksell, Stockholm, 1975)
[10] H. Armon, E.R. Bauminger, A. Diamant, I. Nowik and S. Ofer, Nucl. Phys. A233 (1974) 385;
M. Neiman, R. Kalish, D.R.S. Somayalulu, B. Herskind, F. Genovese and L. Grodzins, Phys. Lett. 52B (1974) 189;
C.W. Towsley, D. Cline and R.N. Horoshko, Nucl. Phys. A250 (1975) 381;
R. Graetzer, S.M. Cohick and J.X. Saladin, Phys. Rev. C12 (1975) 1462;
P.B. Vold, D. Cline, J. Sprinkle and R. Scharenberg, Bull. Am. Phys. Soc. 21 (1976) 581;
P. Paradis, G. Lamoureux, R. Lecomte and S. Monaro, Phys. Rev. C14 (1976) 835;
M.T. Esat, D.C. Kean, R.H. Spear and A.M. Baxter, Nucl. Phys. A274 (1976) 237;
R. Lecomte, P. Paradis, J. Barrette, M. Barrette and G. Lamoureux, Nucl. Phys. A284 (1977) 123;
M.P. Fewell, D.C. Kean, R.H. Spear and A.M. Baxter, J. Phys. G3 (1977) L27;
J.J. O'Brien, J.X. Saladin, C. Baktash and J.G. Alessi, Phys. Rev. Lett. 38 (1977) 324;

[10] continued
C. Baktash, J.X. Saladin, J.J. O'Brien and J.G. Alessi, Bull. Am. Phys. Soc. 22 (1977) 546
[11] M. Sakai, Atomic and Nucl. Data 15 (1975) 513
[12] L. Grodzins, Phys. Lett. 2 (1962) 88
[13] M.A.J. Mariscotti, G. Scharff-Goldhaber and B. Buck, Phys. Rev. 178 (1969) 1864
[14] C.E. Bemis, F.K. McGowan, J.L.C. Ford, W.T. Milner, P.H. Stelson and R.L. Robinson, Phys. Rev. C8 (1973) 1466
[15] P. Patnaik, R. Patra and L. Sapathy, Phys. Rev. C12 (1975) 2038
[16] J.F.R. May, V.V. Pashkevich and S. Frauenhofer, Phys. Lett. 68B (1977) 113
[17] V. Paar, in: Problems of Vibrational Nuclei (ed. Alaga, Paar and Šips, North Holland, Amsterdam, 1975)
[18] W. Eyrich, A. Hofmann, U. Scheib, S. Schneider, F. Vogler and H. Rebel, Phys. Lett. 63B (1976) 406 and Nucl. Phys. A287 (1977) 119

PART B (EXPERIMENT)

CHAPTER III

THE USE OF SINGLE-CRYSTAL IRON FRAMES IN TRANSIENT FIELD MEASUREMENTS

1. Introduction

Magnetic dipole moments of excited states may provide a sensitive test for nuclear models, even if they can only be determined with an accuracy of 10-20 %. Most of the higher excited states, however, have short lifetimes (τ_m < 10 ps) so that their magnetic moments cannot be measured by conventional experimental techniques, if at all. The most powerful method for g-factor measurements on excited states with lifetimes in the region $\tau_m \approx 0.1 - 10$ ps is the transient field implantation perturbed angular correlation (TF-IMPAC) technique [1, 2]. In this method excited and aligned nuclei, produced by a nuclear reaction, are recoiled into a magnetized ferromagnetic medium. During the slowing down the nucleus experiences a transient magnetic field, which through the interaction with the nuclear magnetic moment causes the spins of the excited nuclear state to precess. This precession is observed as a rotation of the angular distribution of the deexciting γ-rays. The measured rotation is an integral over the slowing-down history weighted by the nuclear decay probability. If the calibration of these dynamical fields as a function of recoil velocity and atomic number of the moving ion is known, the g-factor of the excited state can be extracted from the observed precession. In this chapter we will only consider experimental procedures and the calibration problem is deferred to the next chapter (see also [3]).

2. Magnetization of the ferromagnetic backing

In TF-IMPAC experiments the penetration depth of the recoiling ions in the ferromagnetic backing is typically 1-5 μm. It is therefore of considerable importance to know the surface magnetization properties. In most of the transient field experiments performed so far polycrystalline Fe target backings have been used. As has been shown [4] there may be a striking difference between the surface and bulk magnetization at low magnetizing fields. This phenomenon, a distinctive lag in the surface magnetization, is probably due to demagnetizing fields at the surface. For full surface magnetization external fields of more than 1 kgauss are necessary. This inevitably causes a non-negligible fringing field near the target, which has the following effects. Firstly the beam of incoming particles is bent in the fringing field, which turns the reference axis. Secondly, since γ-rays are always detected in coincidence with outgoing reaction particles at an average angle of 180° to the beam direction, the real mean detection angle is different from 180°. This off-axial detection causes a change in the magnetic substate populations of the nuclear state which is observed as a rotation of the angular correlation [2]. This beam-bending effect is not calculable except for pure Coulomb excitation. It must therefore be measured independently with a non-ferromagnetic backing in order to obtain the real transient field rotation angle. Since the experimental conditions for the two measurements should be identical the resulting experimental errors are approximately equal. Hence the total measuring time required for a given error in the net rotation is four times as long as it would be in the absence of the beam-bending effect.

We will present a method to circumvent the problems associated with beam bending. The possibility to use a single-crystal iron frame as a target backing will be discussed in detail. Preliminary results have been reported elsewhere [5]. Integral precession measurements on several nuclei with the single-crystal backing will be compared with results obtained with the conventional set-up. The possibility to use thin foils (2-5 μm) of ferromagnetic material will briefly be touched upon. It will be shown through the magneto-

optical Kerr effect [6], that both the single-crystal Fe frames and the thin foils can be magnetized completely at fairly low fields, for which the corresponding fringing fields are negligible.

3. Surface magnetization measurements

3.1. THE MAGNETO-OPTICAL KERR EFFECT

When a beam of linearly polarized light is incident on a metallic surface the reflected beam will also be linearly polarized, if the plane of polarization is either perpendicular or parallel to the plane of incidence (defined by the incoming light beam and the normal of the surface). This is no longer true, however, when the reflecting surface is magnetized [6]. Then the reflected beam is, in general, elliptically polarized, the degree of ellipticity being proportional to the surface magnetization. Three cases can be distinguished, depending on the orientation of the magnetization relative to the reflecting plane and the plane of incidence [4].

(i) The polar effect. The magnetization direction is perpendicular to the surface. Though the effects are the largest in this case it is of no use for our purpose, since it is not the configuration used in TF-IMPAC experiments.

(ii) The transverse effect. The magnetization direction is in the reflecting plane, perpendicular to the plane of incidence. No rotation of the plane of polarization occurs.

(iii) The longitudinal effect. In this case the magnetization direction is both in the reflecting plane and the plane of incidence. The effect attains its optimum at an angle of incidence of about 60°. The rotation is proportional to the magnetization and reaches a maximum of about 5' for Fe.

The magneto-optical Kerr effect (MOKE) is particularly suited for surface magnetization studies. It probes the outer layers of atoms in a sample. For a wavelength of e.g. 0.6 μm the average penetration depth of the incident light is 12 nm which corresponds to about 40 layers of atoms. Thus, if induction measurements of the bulk magnetization as well as MOKE measurements of the surface in-

dicate saturation, one may readily assume saturation along the whole trajectory of the recoiling ions in the ferromagnetic medium. The maximum Kerr effect is reached at the point of saturation, whilst magnetic flux measurements must always be corrected for the external field contribution. The main disadvantage of the Kerr technique is that the metallic surface has to be very clean. The presence of non-ferromagnetic oxides may obscure the effect completely. This eliminates effectively the possibility of an absolute measurement of the magnetization.

The interaction of implanted radioactive nuclei with the static magnetic hyperfine field in the ferromagnetic medium has been used as an alternative to study the surface magnetization [7]. These local fields, however, may not always reflect the total magnetization of the medium, so that this method, apart from being time consuming, is not considered very reliable.

3.2. SET-UP

The experimental set-up used for the MOKE measurements is schematically shown in fig. 1. The light beam from a He-Ne laser passes through a Glan-Tompson prism polariser (polarization direction perpendicular to the plane of drawing). Subsequently a part of the beam is split off by a semi-mirror (SM1) to serve for reference purposes.

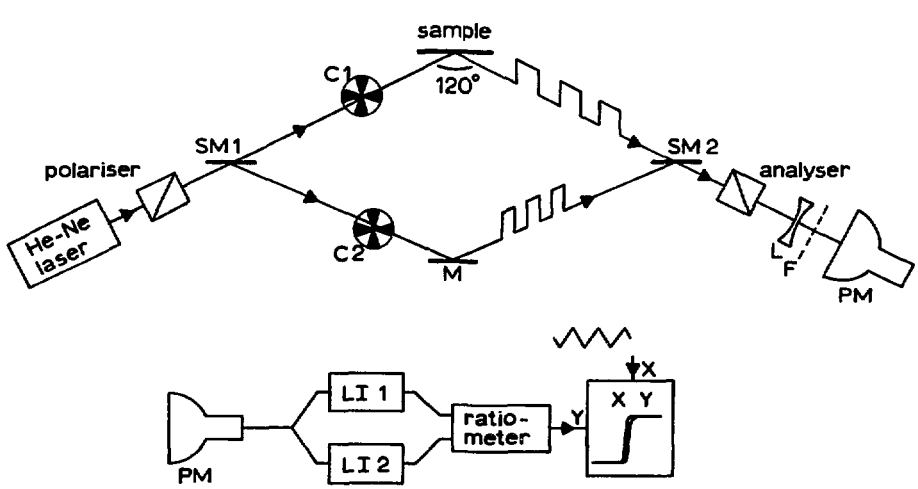

Fig. 1. A schematic representation of the MOKE set-up.

The main beam is incident on the sample (to be magnetized in longitudinal direction) over a total area of 1 mm x 2 mm. The reference beam is united with the reflected main beam through a mirror (M) and a semi-mirror (SM2). Both beams are detected after passing an analyser prism in a photomultiplier (PM) which is protected against local over-radiation by a defocussing lens (L) and a colour filter (F). In order to separate the reference beam and the beam reflected from the sample, the reference and incident beams pass through choppers (C1 and C2) run at different frequencies. The signal from the photomultiplier is fed to two lock-in amplifiers (LI1 and LI2) which are tuned to the respective chopper frequencies. These frequencies are adjusted such that cross-talk is minimized. Finally the ratio of the output signals of the lock-in amplifiers is fed to the y-input of an XY-recorder. Its x-input is driven by a signal proportional to the external magnetic field strength applied to the sample.

The laser, the prisms, the semi-mirrors, chopper 1 and the photomultiplier are mounted on two optical benches. The angle between the rails is 120° and the sample holder is placed at the rail intersection. The following steps are involved in the optical alignment.

(i) The sample is mounted with its reflecting surface perpendicular to the beam (angle of incidence of $\theta = 0^{\circ}$).

(ii) The sample is rotated to the optimum angle of incidence of $\theta = 60^{\circ}$ at which the photomultiplier output has a maximum.

(iii) The polariser and analyser are adjusted such that the light incident on the sample is polarized perpendicularly to the plane of incidence and the photomultiplier output has a minimum (polariser and analyser crossed).

(iv) The analyser prism is finally rotated over 1° to generate sufficient light to linearize the photomultiplier output signal as a function of magnetization.

The MOKE set-up is insensitive to intensity variations in the laser beam (as large as 30 %) and to changes in sensitivity of the photomultiplier. Other than most optical devices it can be used in daylight. A typical magnetization curve is shown in fig. 1 in which the direct output of the XY-recorder is presented (for details we refer to subsect. 3.3). Only small irregularities, probably due to noise in the associated electronics, can be observed. MOKE ex-

periments on two single-crystal Fe frames and a polycrystalline frame for comparison as well as measurements on thin foils (2-3 μm) of Fe, Co and Ni are discussed below.

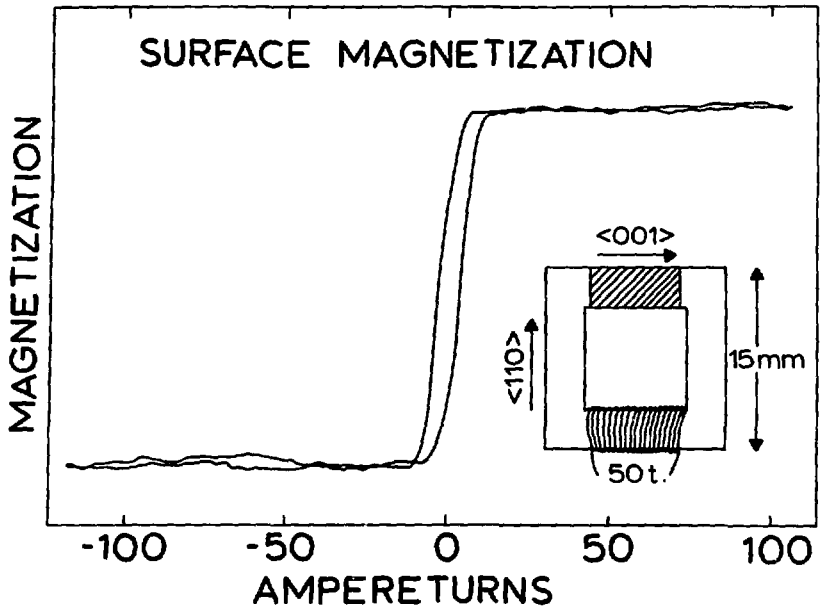

Fig. 2. An example of a hysteresis curve obtained in a MOKE measurement on the <001> leg of crystal 1. In the insert the details of this crystal are shown. The laser beam was incident on the hatched area.

3.3. RESULTS

The iron window frames which were investigated all have 1 mm thickness, outside dimensions of 14 mm x 14 mm and sides of 3 mm wide. Two of the frames are single (α-Fe, cubic) crystals which were produced at Groningen University. They were made by the strain anneal method [8], cut by spark erosion and polished and annealed afterwards. The polycrystalline frame was made of armco-iron. Single crystal 1 has two of its sides parallel to within 30' to the <001> crystal axis (a direction of easy magnetization see e.g. [9]) and two parallel to the <110> axis (see insert in fig. 2). Single crystal 2 has two sides approximately parallel to the <100> axis and two approximately in the <010> direction. The plane of the frame, however, is at an angle of 4° with the (001) crystal plane. Coils

of 50 turns around one of the legs were used to magnetize the frames. For such a configuration, one ampereturn corresponds to a magnetizing field of about 0.3 gauss (24 A/m). An example of a MOKE measurement on the <001> leg of single crystal 1, is shown in fig. 2. A triangularly varying current with a period of 4 min was applied to the coil. The corresponding magnetizing field changes slowly enough to avoid skin effects. It is interesting to note that the magnetization curve shown in fig. 2 was taken on a spot which had been bombarded with a beam of 35 MeV $^{12}C^{5+}$ ions during a period of 150 h at a current of 100 nA.

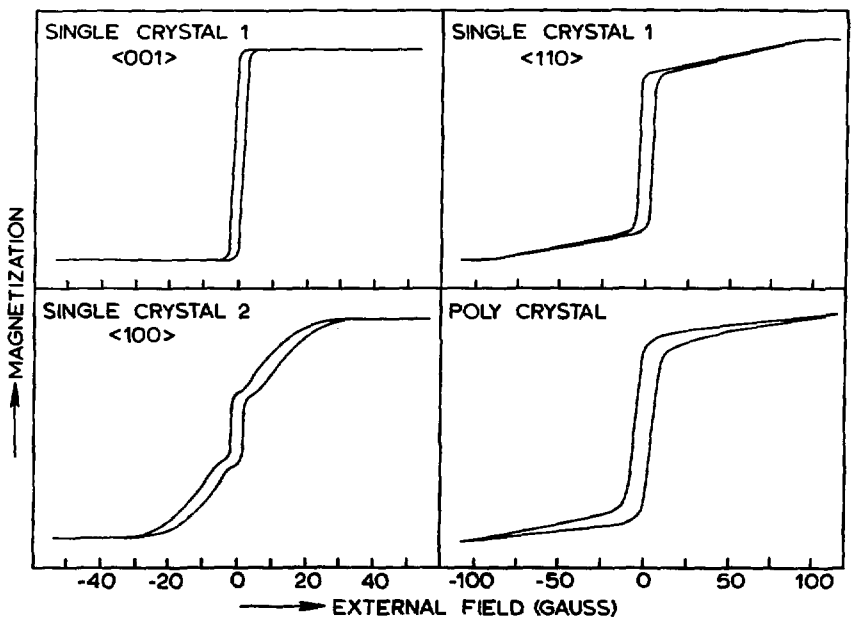

Fig. 3. The results of MOKE measurements on the three iron frames.

The MOKE results for the three window-frames are summarized in fig. 3. The curves represent averages over about 10 periods of the external field in order to eliminate the small and unsystematic irregularities. The magnetization in the <001> direction for single crystal 1 shows an almost perfect hysteresis curve. Saturation is reached at already 3 G. The MOKE curve for the <110> direction indicates that 70 % of the saturation is reached within 5 G but that full saturation is only obtained at about 100 G. For single crystal

2 a peculiar behaviour is found in the surface magnetization. Full saturation is attained at an external field of about 30 G. The MOKE measurement on the polycrystalline frame shows that no saturation is obtained even at 100 G, although an appreciable fraction of the saturation magnetization is reached with an external field of only 20 G. This frame was also investigated with fast pulsed magnetizing currents corresponding to fields up to 400 G. These measurements indicate that full saturation is only obtained above 300 G.

From measurements with a small-size Hall probe near the crystal surface and at a magnetizing field of 40 G, an upper limit of 2 G was estimated for the fringing field. This is at least a 100 times as small as in the conventional set-up with a large electromagnet [2]. This means that beam-bending effects at 40 G are negligible indeed. Hence both single crystals may be considered useful as a target backing in TF-IMPAC experiments.

Magnetic induction measurements of the bulk magnetization of the window frames have also been performed. For both single crystals the resulting hysteresis curves showed a behaviour identical to the MOKE curve of the surface in the <001> direction of single crystal 1 (upper left corner in fig. 3). For the polycrystalline frame the bulk and surface hysteresis curves coincided within the limits of the experimental accuracy.

Our findings support the tentative conclusion [4] that the observed lag in the surface magnetization of single-crystal and polycrystalline Fe strips is due to demagnetizing fields owing to the open ends. In closed frames this effect is absent. The distinct lags in the surface magnetization in the <110> direction of single crystal 1 and in single crystal 2 are of different origin. In these cases the direction of easy magnetization does not coincide with the sides of the frame. This gives rise to small domains with a magnetization opposite to the field direction ("fir-tree" patterns, see e.g. [9]).

Finally we briefly mention the results of MOKE measurements on thin foils (2-3 μm) of Fe, Co and Ni. Such foils may be advantageous in transient field experiments for a number of reasons (see also

[10]). Polycrystalline foils are easily available, cheaper and less vulnerable than single-crystal frames. They also allow experiments in which reaction particles are detected at forward angles or in which the recoiling nuclear ions are stopped outside the foil in a non-ferromagnetic backing. The latter possibility eliminates the need for (often unknown) static magnetic hyperfine field corrections to the measured precession. A disadvantage of foils is that the density may differ from that of the bulk, so that an additional calibration may be necessary.

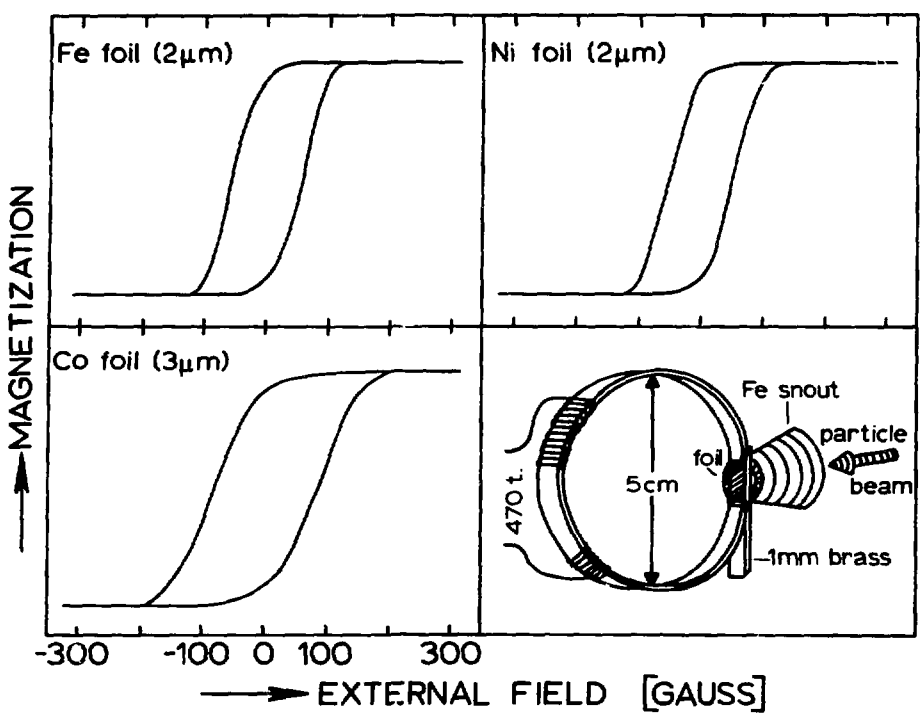

Fig. 4. The results of MOKE measurements on thin Fe, Co and Ni foils. The electromagnet used to magnetize the foils and the Fe snout to shield the fringing field are also shown.

The smoothened MOKE hysteresis curves obtained are displayed in fig. 4. As can be seen saturation is reached for Fe and Ni within 120 G and for Co at 200 G. The small electromagnet used to magnetize the foils and the Fe snout for shielding the fringing field

are also shown. With this snout the fringing field was estimated to be six times as small as in the conventional set-up [2].

4. Application to transient field IMPAC measurements

In this section we describe a number of TF-IMPAC integral precession measurements to test the single-crystal frames. The results obtained with these frames are compared with those obtained in the conventional set-up.

4.1. SET-UP AND INTERPRETATION

The "conventional" set-up used in our laboratory for TF-IMPAC integral precession measurements has been described in detail in [2]. The associated data collection system, which includes a CDC 1700 on-line computer, has been described in [11]. We only mention the details relevant to the present work.

Outgoing reaction particles are commonly detected in a 200 μm thick annular Si surface barrier detector, which subtends angles between 166° and 173°. Gamma-radiation coincident with particles is detected in four 12.7 cm diam. by 12.7 cm long NaI(Tl) detectors at angles of $\pm 72^{\circ}$ and $\pm 108^{\circ}$ to the beam direction in the horizontal plane and at a distance of 20 cm from the target. Targets are evaporated on polycrystalline Fe strips with thickness of 5 or 10 μm. These strips are magnetized in a field of 1.5 kG (0.15 T) generated by an electromagnet. The magnetization direction is reversed automatically every 2 min to avoid systematic effects.

For the present measurements the electromagnet and accompanying target holder are replaced by a single-crystal Fe frame with the magnetizing coil and the target. Owing to the absence of the return yoke of the electromagnet two additional NaI(Tl) counters were positioned at $\pm 18^{\circ}$ to improve statistics. The target material is deposited on the centre part of one of the legs of the frame parallel to the <100> or an equivalent direction. This side is then placed vertically in the target chamber such that the incoming beam is perpendicular to the frame to within a few degrees. The heat conduction to the frame support is sufficiently good to avoid excessive heating

of the frame by the beam.

The integral spin precession angle is deduced from the rotation angle of the γ-ray angular correlation. For this purpose coincident γ-rays are collected at the afore-mentioned detection angles of $\pi/2\ (n \pm 1/5)$ with $n = 0, \pm 1$, which are optimum for correlations of a fully aligned 2^+ state [2]. The mean integral precession angle $\Delta\theta$ can be expressed as

$$\Delta\theta = \frac{\sqrt{r} - 1}{\sqrt{r} + 1} \cdot \left[\frac{1}{W(\theta)} \frac{dW(\theta)}{d\theta}\right]^{-1}, \tag{4.1}$$

where $W(\theta)$ represents the angular correlation function. The double ratio r and the corresponding effect ε are defined by

$$r = 1 + \varepsilon = \frac{N[\frac{\pi}{2}(n+\frac{1}{5})]\uparrow}{N[\frac{\pi}{2}(n+\frac{1}{5})]\downarrow} \cdot \frac{N[\frac{\pi}{2}(n-\frac{1}{5})]\downarrow}{N[\frac{\pi}{2}(n-\frac{1}{5})]\uparrow}, \tag{4.2}$$

where $N[\phi]\uparrow\downarrow$ denotes the number of coincident counts accumulated in the γ-ray detector at angle ϕ with magnetic field up or down. For the four γ-ray detectors at $\pm 72^\circ$ and $\pm 108^\circ$, the cross effect ε_c, given by

$$\varepsilon_c = \frac{N[\frac{\pi}{2}(1\pm\frac{1}{5})]\uparrow}{N[\frac{\pi}{2}(1\pm\frac{1}{5})]\downarrow} \cdot \frac{N[-\frac{\pi}{2}(1\mp\frac{1}{5})]\downarrow}{N[-\frac{\pi}{2}(1\mp\frac{1}{5})]\uparrow} - 1, \tag{4.3}$$

can be used as a check on the measurement. This cross effect should be zero.

The calibration of the double ratio r against rotation angle was obtained in the present work by measuring ε for a rotation of 2°. This was performed by off-setting the sixcounter array by $\pm 2^\circ$ with the magnetic field set to zero. This procedure is to be preferred over that used in the past. In the latter the complete angular correlation function was measured and fitted by the usual even-order Legendre polynomial series. The coëfficients of this series were

then used to calculate the logarithmic derivative $W^{-1}\ dW/d\theta$.

4.2. RESULTS AND DISCUSSION

Transient field precession measurements were performed on the first-excited 2^+ states of ^{28}Si, ^{20}Ne and ^{12}C. The reasons for selecting these cases are discussed below.

(i) The first-excited state of ^{28}Si was chosen because it is typical for most low-velocity measurements with light projectiles. This case has also provided the cleanest, fastest and most accurate of all transient field measurements performed with a conventional set-up [12].

(ii) The case of ^{20}Ne is typical for a high-velocity measurement with energetic heavy particles. Large precessions are expected since the transient field increases with recoil velocity [13]. Since the ^{20}Ne ions are produced in the heavy-ion $^{12}C(^{12}C, \alpha)$ reaction this case may also provide a good test on possible radiation damage of the single-crystal lattice.

(iii) For the first-excited 2^+ state of ^{12}C a reasonably accurate TF-IMPAC result has been obtained by the Bonn-Strasbourg group [14] by the conventional method. Because the lifetime of this state is very short, $\tau_m = 65 \pm 3$ fs [15], this case tests the single-crystal surface magnetization best. The average probing depth amounts only 0.4 μm.

The details relevant to the experimental conditions in these measurements are summarized in table 1. For ^{28}Si two measurements were performed with single crystal 1. In the first (see also [5]) a magnetizing field of 3 G was applied, just sufficient for saturation (see fig. 3), whereas in the second 40 G was taken. For ^{20}Ne first a measurement with single crystal 2 as a target backing and subsequently a (shorter) measurement with single crystal 1 were performed, both at a magnetizing field of 40 G. In the experiment on $^{20}Ne(2_1^+)$ with the conventional set-up the targets were deposited onto 10 mg/cm^2 thick pure Fe and 0.25 μm thick Ag backings for the effect and beam-bending measurements, respectively. For ^{12}C only one TF-IMPAC measurement was performed with single crystal 1 at a magnetizing field of 40 G.

It can be inferred from table 1 that the results with the con-

Table 1

Summary of the experimental conditions and observed integral precessions for the ^{28}Si, ^{20}Ne and ^{12}C measurements and a comparison to previous results

Nucleus (E_x[MeV]; τ_m[ps])	Reaction	Beam E[MeV], I[nA]	Target [a] d[μg/cm^2]	Single-crystal [b] t[h]	Single-crystal [b] Δθ[mrad]	Conventional [b,c] t[h]	Conventional [b,c] Δθ[mrad]
^{28}Si (1.78; 0.70)	$^{28}Si(\alpha, \alpha')$	7.50; 80 (He^+)	170	30	1.40 ± 0.09	106	1.42 ± 0.15
		45 (He^+)		19	1.43 ± 0.15		
^{20}Ne (1.63; 1.04)	$^{12}C(^{12}C, \alpha)$	35.4 ; 70 (C^{5+})	200	45	4.8 ± 0.8	90	4.4 ± 1.2
		60 (C^{5+})		30	4.6 ± 1.0		
^{12}C (4.43; 0.06)	$^{12}C(\alpha, \alpha')$	10.2 ; 50 (He^{++})	20	70	0.65 ± 0.13	≈340	0.85 ± 0.14
						≈100	0.71 ± 0.25

a) Natural elemental targets were used.

b) The symbols t and Δθ stand for measuring time and precession angle, respectively.

c) The ^{28}Si result is from [12]; the ^{12}C results are from [14].

ventional set-up and those obtained with the single-crystal backings agree well. From the ^{28}Si experiments we conclude that it suffices to apply a magnetizing field which, from the MOKE measurements, was found to be just sufficient for saturation. Apparently the saturation properties do not deteriorate under beam conditions. The ^{20}Ne results indicate that the crystals withstand a heavy-ion beam. The data for crystal 2 (first measurement) also imply that even a non-perfect frame (see subsect. 3.3 and fig. 3) can be used. Finally, from the ^{12}C data it is clear that indeed the very surface of the single crystal frame is well magnetized.

From the measuring times given in table 1 the time gain which is attained with single-crystal backings is obvious. Part of this gain is due to the increased number of detectors (six instead of four).

Although the results of the TF-IMPAC measurements prove satisfactory it may be worthwhile to consider the possibility of radiation damage in some detail. Such damage will mainly be caused by the incident beam. There may also be a small contribution from the slowing-down ions. In any case most damage occurs at the end of the trajectory of the projectiles or the recoiling ions, i.e. where the nuclear stopping power dominates. This prevents the possible detection of radiation damage after an IMPAC experiment by a MOKE measurement since the penetration depth of the laser light ($\approx$ 10 nm) is only a small fraction of the range of the projectiles or ions (1-10 μm).

The TF-IMPAC integral precession measurements were analysed in some ten consecutive time intervals to detect a possible decrease in the precession angle. This procedure was meaningful for the Si and C measurements. For the Ne measurements unfortunately the errors are quite large so that a change of the precession angle is virtually undetectable. In fig. 5 the time-dependent results for ^{28}Si are shown. A least-squares fit with an assumed linear time dependence yields a slope of $+0.02 \pm 0.02$ mrad/h. For ^{12}C also no significant change of the precession angle with time was observed and the ^{20}Ne data are consistent with no decrease.

It may after all not be so surprising that radiation damage effects are small for the following reasons.

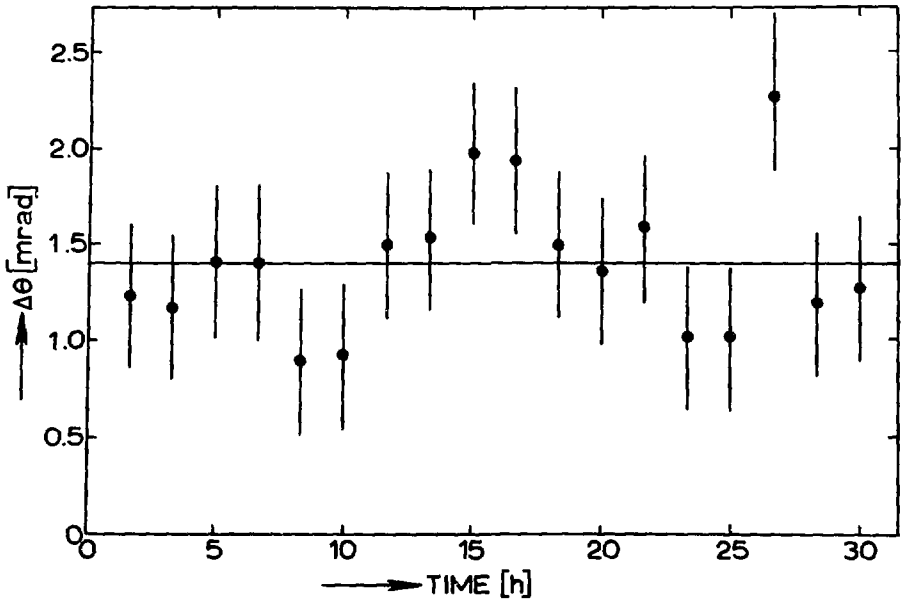

Fig. 5. The measured rotation angle of the angular correlation for the first ^{28}Si experiment as a function of time. Each point corresponds to a measuring time of 100 min. The line represents the average value.

(i) The incident particles are generally stopped way beyond the penetration depth of the ions, except perhaps in heavy-ion reactions, so that the ions do not traverse a damaged region.

(ii) The transient field is proportional to the ion velocity. Therefore most of the rotation takes place at the beginning of their trajectory where no damage is expected.

(iii) The concentration of implanted ions is usually rather low. For most cases this is considerably less than one per 10^6 Fe atoms integrated over the total experimental time.

(iv) Often the lifetime of the excited state of the recoiling nucleus is less than the stopping time so that there are no contributions from the end of the ion's trajectory.

5. Conclusion

Since it is generally so that the surface of a ferromagnet is more difficult to magnetize than the bulk, the magneto-optical Kerr effect, with a probing depth of only some 10 nm, yields a good measure of the saturation of a ferromagnetic backing for transient field experiments. It has been shown in a number of transient field experiments that if the Kerr results prove satisfactory also the measured integral precession angles agree with previously obtained values.

A considerable improvement of the transient field method to determine g-factors has been obtained by the use of single-crystal iron frames as target backings. These frames can be fully magnetized at low external fields so that fringing fields are negligible. This yields a gain of a factor of four to six in measuring time. No indication for radiation damage effects has been found. The large reduction in measuring time enables one to perform more difficult experiments, e.g. on states with a much shorter lifetime or for cases with a less anisotropic γ-ray distribution.

There are two disadvantages associated with the use of the (rather thick) single-crystal frames. It is impossible to detect outgoing reaction particles at forward angles and the background with high-energy light incident particles (protons or α-particles) is prolific. These problems can be circumvented by the use of thin backings. Measurements of the Kerr effect on thin (few μm) ferromagnetic foils indicate that at relatively low magnetic fields full saturation is obtained. For these foils the fringing fields are then also sufficiently low so that beam-bending measurements are not necessary.

References

[1] G.K. Hubler, H.W. Kugel and D.E. Murnick, Phys. Rev. Lett. 29 (1972) 622 and Phys. Rev. C9 (1974) 1954

[2] J.L. Eberhardt, R.E. Horstman, H.W. Heeman and G. Van Middelkoop, Nucl. Phys. A229 (1974) 162

[3] P.C. Zalm, A. Holthuizen, J.A.G. De Raedt and G. Van Middelkoop, Phys. Lett. 69B, (1977) 157

[4] H. De Waard, E. Uggerhøj and G.L. Miller, J. Appl. Phys. 46 (1975) 2264
[5] P.C. Zalm, J.L. Eberhardt, R.E. Horstman, G. Van Middelkoop and H. De Waard, Phys. Lett. 60B (1976) 258
[6] J. Kerr, Philos. Mag. 3 (1877) 321
[7] B. Skaali, R. Kalish and B. Herskind, Hyp. Int. 1 (1976) 381
[8] R.A. Landise, The Growth of Single Crystals (Prentice Hall, Englewood Cliffs, N.J. 1971) p. 133
[9] S.V. Vonsovskii, Magnetism, Vol. 2 (Wiley, New York, 1974)
[10] J.C. Adloff, J. Gerber, M.B. Goldberg, W. Knauer, G.J. Kumbartzki and K.-H. Speidel, reported at: Hyperfine Interactions IV (Madison, 1977)
[11] R.E. Horstman, J.L. Eberhardt, H.A. Doubt, C.M.E. Otten and G. Van Middelkoop, Nucl. Phys. A248 (1975) 291
[12] J.L. Eberhardt, R.E. Horstman, H.A. Doubt and G. Van Middelkoop Nucl. Phys. A244 (1975) 1
[13] J.L. Eberhardt, R.E. Horstman, P.C. Zalm, H.A. Doubt and G. Van Middelkoop, Hyp. Int. 3 (1977) 195
[14] M.B. Goldberg, G.J. Kumbartzki, K.-H. Speidel, M. Forterre and J. Gerber, Hyp. Int. 1 (1976) 429;
M.B. Goldberg, E. Konejung, W. Knauer, G.J. Kumbartzki, P. Meyer and K.-H. Speidel, Phys. Lett. 58A (1976) 269
[15] F. Ajzenberg-Selove, Nucl. Phys. A248 (1975) 1

CHAPTER IV

VELOCITY AND ATOMIC NUMBER DEPENDENCE OF THE TRANSIENT MAGNETIC FIELD IN IRON

1. Introduction

The transient magnetic field experienced by nuclei during their slowing down in polarized ferromagnetic material has been used to determine g-factors of short-lived ($\tau_m \simeq 1$ ps) excited nuclear states [1, 2]. Such a field causes by the interaction with the nuclear magnetic moment a spin precession of an aligned (excited) nuclear state. This precession is observed as a rotation of the angular distribution pattern of the deexciting γ-rays on implantation of the ion into a ferromagnet (see chapter III). The dynamical behaviour of the transient field must be known in order to extract g-factors from measured precession angles because the observed rotations represent an integral over the slowing-down history folded with the lifetime of the nuclear state.

In the past the transient field was estimated from the Lindhard and Winther (LW) theory [3], in which the field is described by an enhancement of the (polarized) electron density at the moving nucleus due to Coulomb scattering on the slowing-down ion. The LW theory predicts essentially linear dependences of the transient field on the atomic number Z of the ion and the inverse of the ion velocity. The LW theory could at the time explain most of the existing experimental data by introducing an effective average polarized electron velocity. Discrepancies were only observed for ^{56}Fe [4] and ^{196}Pt [5] recoiling into magnetized Fe; too high precessions were found at high velocities. These discrepancies were, however, attributed to radiation damage. Later similar deviations from the LW theory were found also for light ions [6, 7].

The first systematic investigation of the velocity dependence of the transient field was carried out in our laboratory for ^{28}Si

recoiling into Fe [8]. In this experiment an increase of the observed integral precessions with initial recoil velocity was found. The data are consistent with an assumed linear velocity dependence of the transient field [8]. These findings were confirmed by a reinvestigation of ^{56}Fe recoiling into polarized Fe [9]. The data seemed also consistent with a linear dependence of the transient field on the atomic number Z of the ion [8], although for $Z < 9$ deviations from the linear Z-dependence were observed.

The measured large integral precession angles at high recoil velocity, which indicated an anomalous enhancement of the transient field over the LW estimate, were interpreted in a microscopic model [8]. In this model it is assumed that, due to frequent collisions in the solid, vacancies are produced in inner electronic s-shells of the moving ion followed by capture of polarized electrons from the ferromagnetic backing. The superposition of the atomic and LW fields could account for all available data semi-quantitatively. For e.g. ^{28}Si, the transient field was thought to be mainly due to polarized 2s and 1s electrons for velocities $v \leq 4v_o$ and $v > 4v_o$ ($v_o = c/137$), respectively.

In this chapter we present the results of transient field implantation perturbed angular correlation (TF-IMPAC) experiments on the first-excited 2^+ states of ^{20}Ne and ^{24}Mg recoiling into Fe. Integral precession measurements were performed with several nuclear reactions, yielding initial recoil velocities up to $v \approx 8v_o$, to test further the linear velocity dependence. The present results, along with existing data, lead to an empirical calibration of the transient field in Fe for $Z \lesssim 26$. The Z-dependence exhibits a marked atomic shell structure, which has led to a better insight in the microscopic "polarized electron capture"(PEC) model.

2. Experimental procedure and results

Ions of ^{20}Ne and ^{24}Mg in their first-excited nuclear states were produced by various reactions and implanted into magnetized Fe. Integral spin-precession angles were deduced from γ-ray counts accu-

mulated in six NaI(Tl) detectors positioned at angles $\pi(n \pm 1/5)2$ $n = 0, \pm 1$, with respect to the incident beam, and for magnetization direction up and down. Gamma radiation was detected in coincidence with outgoing reaction particles detected at backward angles. Details of the experimental set-up and the method of analysis for the TF-IMPAC measurements are described in chapter III sect. 4 (and references contained therein). Some details of the present experiments and the results are given below.

2.1. THE ^{20}Ne EXPERIMENTS

The first-excited 2^+ state at 1.63 MeV (τ_m = 1.0 ps) was populated by the $^{12}C(^{12}C, \alpha)^{20}Ne^*$ reaction at three ^{12}C bombarding energies. Resonances in the yield and γ-ray anisotropy were found at incident energies of 14.0, 18.2 and 35.4 MeV. These energies correspond to initial recoil velocities for ^{20}Ne of v_i/v_o = 5.2, 5.9 and 7.8 for α-particle detection at 180°. For the first two experiments targets with a thickness of 50 μg/cm^2 natural C, sputtered onto one of the legs of a single-crystal Fe frame, were used. The beam currents of $^{12}C^{3+}$ and $^{12}C^{4+}$ ions were kept at 100 nA during the experiments. The measuring time for each experiment was 52 h. The highest velocity measurement was divided into three separate experiments in order to check the properties of two single-crystal frames against the conventional target set-up. The relevant details for this measurement are given in chapter III.

2.2. THE ^{24}Mg EXPERIMENTS

The 2_1^+ level at 1.37 MeV (τ_m = 2.0 ps) was populated by the $^{24}Mg(\alpha, \alpha')$, $^{16}O(^{12}C, \alpha)$ and $^{12}C(^{16}O, \alpha)$ reactions. The bombarding energies were $E(He^{++})$ = 18.8, $E(^{12}C^{3+})$ = 17.0 and $E(^{16}O^{6+})$ = 38.4 MeV. This leads to initial recoil velocities for the ^{24}Mg ions of v_i/v_o = 3.7, 5.1 and 7.7, respectively. In the (α, α') experiment it proved impossible to use a single-crystal frame as a target backing due to a prolific γ-ray background caused by competing reactions in the 1 mm thick frame. Instead the conventional set-up with a large electromagnet was used, with targets of natural Mg, with thicknesses of 165 μg/cm^2 and 250 μg/cm^2, evaporated on 5 μm thick Fe and 10 μm Ag strips for the precession and beam-bending (see chapter III) measurements, respectively. In a total measuring time

of 70 h with a beam current limited to 30 nA a rather inaccurate result was obtained. For the other two experiments targets with thicknesses of 300 μg/cm^2 WO_3 and 50 μg/cm^2 natural C were used, evaporated and sputtered onto single-crystal Fe frames. The beam currents were kept at 100 nA and beam times of 60 and 30 h were used for the intermediate and high velocity experiments, respectively.

2.3. RESULTS

A summary of the measured integral precession angles is given in table 1. The angles $\Delta\theta$ were determined from the ratios of coincident counts accumulated in the γ-ray detectors with magnetic field up and down as described in chapter III.

The frequency distributions of the effects ε and cross effects ε_c as well as the time evolution of the mean precession angle, per recorded magnetic tape, served as a consistency check on the data (see also chapter III). No significant deviation from purely statistical distributions was observed in any of the cases.

Table 1

Summary of the measured integral precession angles $\Delta\theta$ for $^{20}Ne(2_1^+)$ and $^{24}Mg(2_1^+)$

Nucleus	Reaction	$E_{incident}$ [MeV]	v_i/v_o	$\Delta\theta$ [mrad]
^{20}Ne	$^{12}C(^{12}C, \alpha)$	14.0	5.2	1.8 ± 0.3
	$^{12}C(^{12}C, \alpha)$	18.2	5.9	2.5 ± 0.5
	$^{12}C(^{12}C, \alpha)$	35.4	7.8	4.6 ± 0.6
^{24}Mg	$^{24}Mg(\alpha, \alpha')$	18.8	3.7	2.5 ± 1.5
	$^{16}O(^{12}C, \alpha)$	17.0	5.1	4.4 ± 0.8
	$^{12}C(^{16}O, \alpha)$	38.4	7.7	7.3 ± 0.9

3. Systematics of the transient magnetic field in Fe

In this section we investigate the velocity and atomic number dependence of the transient field in iron. For this purpose the presently obtained data are combined with previous results. The implications of the observed, empirically rather simply described, dependences are discussed.

3.1. VELOCITY DEPENDENCE

The precession data in Fe for ^{20}Ne and ^{24}Mg as a function of initial velocity v_i, described in sect. 2, were used to test the linear velocity dependence of the transient field. Therefore the field was parametrized by the simple expression

$$B_{TF}\ (v,\ Z) = C(Z)\ v/v_o, \tag{3.1}$$

where C(Z) depends on the atomic number Z of the moving ion and v is the actual ion velocity (not the intial velocity). The coefficient C(Z) also reflects the properties of the ferromagnetic medium (see subsect. 3.2). The resulting integral precession angle for a certain Z, normalized to g = 1, can then be calculated from the expression

$$\Delta\theta/g = \frac{\mu_N}{\hbar} \int_0^\infty \left[\int_0^{t'} B(t)dt \right] \frac{e^{-\frac{t'+t_i}{\tau_m}}}{\tau_m}\, dt', \tag{3.2}$$

where t_i is the average time that has elapsed before the recoiling ions enter the ferromagnetic backing. The conversion from velocity v to time t is obtained from the electronic and nuclear stopping powers for the moving ions. The electronic stopping powers were taken from the semi-empirical compilation of Northcliffe and Schilling [10] and scaled with recently measured α-particle stopping powers [11]. This procedure yields electronic stopping powers with an es-

timated accuracy of 5 %. For more details about the scaling procedure, as applied in lifetime measurements with the Doppler-shift attenuation method, the reader is referred to [12]. For the nuclear stopping powers a universal expression [13] was used. An uncertainty of 25 % was assigned to these estimates.

The integral in (3.2) is evaluated semi-analytically by the computer program FIELD. For this purpose a continuous function for the stopping power is created by folding a cubic spline through an array of values for electronic plus nuclear stopping powers for a series of ion energies. The inverse of the total stopping power is also approximated by a cubic spline to obtain analytical expressions for time and range.

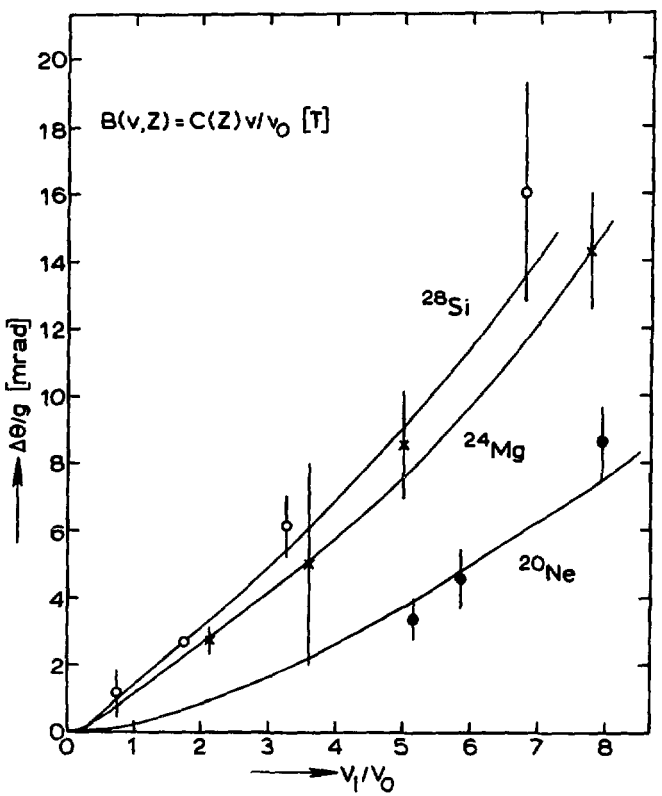

Fig. 1. Measured time-integral precession angles, normalized to g = 1, for the first-excited 2^+ states of ^{20}Ne, ^{24}Mg and ^{28}Si recoiling in iron as a function of initial recoil velocity. The curves correspond to the best fits of an assumed linear velocity dependence of the transient field.

The integral precession angles obtained from the ^{20}Ne and ^{24}Mg experiments, normalized to g = 1, are shown in fig. 1 as a function of the initial recoil velocity v_i along with the data for ^{28}Si [8] and a low-velocity point ($v_i = 2.3\ v_o$) for ^{24}Mg [2]. The g-factors of the first-excited 2^+ states are known to be $g = +0.54 \pm 0.04$ and $g = +0.51 \pm 0.02$ for ^{20}Ne and ^{24}Mg, respectively [14]. For ^{28}Si the g-factor was estimated from the pure $1d_{3/2}2s_{1/2}$ configuration as outlined in chapter I sect. 4 to be $g = +0.53 \pm 0.02$. The curves th ough the points in fig. 1 represent least-squares fits to the data with the field parametrization of (3.1). Normalized goodness-of-fits of $\chi^2 = 1.1$, 0.2 and 0.4 were obtained for ^{20}Ne, ^{24}Mg and ^{28}Si. The contributions of uncertainties in the g-factors and stopping powers were ignored. The constants C(Z) were found to be 70 ± 8, 123 ± 11 and 175 ± 11 [T] for Z = 10, 12 and 14 on the inclusion of the errors in the g-factors and uncertainties in the static fields.

The good fits for ^{20}Ne and ^{24}Mg confirm the earlier observed proportionality of the transient field with recoil velocity for ^{28}Si [8] and ^{56}Fe [9] in iron. Recently this was also found for ^{82}Se in iron and gadolinium [15] and for ^{56}Fe [16] and Gd [17] in magnetized Gd. One may conclude that the linear velocity dependence at least to a certain maximum velocity is a general feature of the transient field.

3.2. ATOMIC NUMBER DEPENDENCE

The coefficients C(Z) obtained for Z = 10-14 together with those extracted from data on lower and higher Z ions in iron can be used to investigate the Z-dependence of the transient field.

For ^{12}C, ^{16}N and ^{18}O only in the case of $^{12}C(2_1^+)$ is the velocity dependence measured [18]. The field increased to $v = 4v_o$ and is close to zero again at $v \approx 9v_o$. For $^{16}N(1_1^-)$ and $^{18}O(2_1^+)$ TF-IMPAC experiments have only been performed at a single initial velocity $v_i < 3v_o$ [6, 7]. In the case of $^{12}C(2_1^+)$ the g-factor was calculated ($g = +0.56 \pm 0.03$ from the pure $p_{3/2}p_{1/2}$ configuration; see chapter I sect. 4) and for $^{16}N(1^-)$ and $^{18}O(2_1^+)$ the g-factors are known experimentally [19]. The field was assumed to be a linear function of velocity at least up to $v = 4v_o$. The C(Z) coefficient for ^{56}Fe in iron was directly obtained from the v-dependent measurements reported in

[9].

The resulting coefficients C(Z) are given in fig. 2. It is clear that the Z-dependence of the transient field is far from a linear function, suggested by the LW theory [3] and the previously obtained empirical formula [8]. Instead a marked atomic shell effect ("saw tooth") is observed, which can be empirically interpreted as follows.

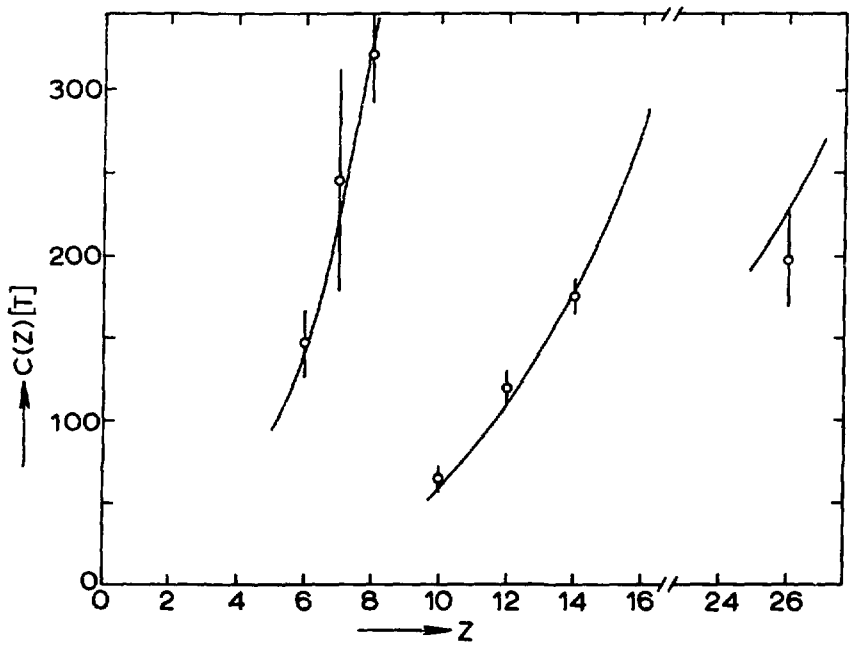

Fig. 2. The atomic number dependence of the transient field in iron. The three curves together correspond to a one parameter fit to the data.

It was assumed that for Z = 6-8, 10-14 and 26 the fields are due to ions with unpaired polarized 1s, 2s and 3s electrons, respectively. The magnetic field of an unpaired electron in the ns subshell at the nucleus is given by [20]

$$B_{ns} = 16.7 \frac{Z(Z-q)^2}{n_{eff}^3} [T], \tag{3.3}$$

where n_{eff} is an effective quantum number [21] close to the principal quantum number n. For the 1s shell one has $n_{eff} = n = 1$, for the 2s subshell n_{eff} is well approximated by $n_{eff} = 2 - 0.8/(Z-1)$ and for the Fe 3s subshell one finds $n_{eff} = 2.67$. The quantity q is a screening charge which represents the total number of electrons in shells within the ns subshell (i.e. q = 0, 2, and 10 for 1s, 2s and 3s shells, respectively). The screening caused by the outer shells is neglected completely. Relativistic corrections and size effects in (3.3) are negligible for $Z \lesssim 30$. Equation (3.3) is the quantum-mechanical analogon of the expression $B_{ns} = 16.7\ Z^3/n^3$ obtained from the semi-classical treatment of hydrogen-like atoms in the Bohr-theory.

The three curves given in fig. 2 are the result of a least-squares fit of the expression

$$C(Z) = \gamma B_{ns} \tag{3.4}$$

to the data. The proportionality constant γ was found as $\gamma = 0.0390 \pm 0.0015$ with a normalized goodness-of-fit of $\chi^2 = 0.7$. The error does not contain a contribution from the uncertainties in the stopping powers. If one would simply take the principal quantum numbers n in (3.3) the quality of the fit is still good ($\chi^2 = 1.4$) and one obtains $\gamma = 0.0422 \pm 0.0016$.

At this point it is worth noting that the fields of unpaired polarized electrons in $np_{1/2}$ and $np_{3/2}$ subshells, which may also contribute to the transient field, are a factor of 8 and 15 weaker than the ns field. Moreover their functional forms are closely similar to that of B_{ns} (3.3) [20] so that they cannot be distinguished experimentally. We have also neglected the Lindhard-Winther field [3] although the underlying theory and basic assumptions are correct. On the inclusion of screening of the moving nucleus by its own electron cloud and the use of the "true" average polarized electron velocity the LW theory predicts fields, however, that are generally small compared to C(Z).

If the description of (3.4) is physically meaningful, one has to conclude first of all that the average number of polarized electrons per ion (causing the transient field) at a given velocity is independent of Z. The second implication is that these electrons are either 1s, 2s or 3s unpaired electrons, depending on the atomic number.

The first conclusion is supported by TF-IMPAC experiments on ^{82}Se [15] and ^{56}Fe [9, 16] recoiling in iron and gadolinium. These data suggest that the transient field at a certain velocity is proportional to the polarized electron density in the ferromagnetic host.

The shell-structure in the Z-dependence is smeared out for Z > 26 (see e.g. the higher-Z data given in [1] . This may be expected as the magnitude of the Z-dependent terms in the size effects, relativistic correction, effective quantum numbers and screening will become increasingly important which tends to smoothen the structure in the Z-dependence. In addition, with increasing Z more electron configurations may contribute to the total field which has a similar effect on the Z-behaviour.

In the next section we will discuss possible explanations for the observed velocity and atomic number dependence within the framework of the microscopic PEC-model.

4. A microscopic interpretation

We have shown in the previous section that the presently available integral precession data provide information on the velocity and atomic number dependence of the transient magnetic field (mainly) in iron. In the empirical description of the Z-dependence the concept of the atomic model, developed by Eberhardt et al. [8], was used implicitly where ionic shells were assumed to be polarized. In this section the atomic model is discussed in view of the new observations. It will be shown that the observed Z-dependence of the transient field in iron can be understood at least qualitatively within this model. There remain, however, some pertinent problems,

the implications of which will be touched upon.

4.1. THE ATOMIC MODEL AND THE v-DEPENDENCE

The atomic model, which is an extension of the first attempts to explain the transient field [22], originates from the fact that the anomalously high fields at high velocities could not possibly be explained by an electron scattering process [8]. The atomic description is based on the notion that, due to the violent and frequent atomic collisions of the moving ion in the ferromagnetic solid, vacancies are produced in inner electronic (s) shells of the ion with high probability. Into these vacancies (polarized) electrons of the magnetized host can be captured. If the cross sections for electron capture (σ_C) and loss (σ_L) for a certain ionic s-(sub)shell are sufficiently high to ensure a (dynamic) equilibrium the fraction y(v) of the ions with only one electron in that shell as a function of velocity v is given by [8]

$$y(v) = \frac{2\sigma_L(v)\sigma_C(v)}{[\sigma_L(v)+\sigma_C(v)]^2} . \qquad (4.1)$$

The loss cross sections are usually taken from the binary encounter approximation (BEA) [23]. The capture cross sections of the loosely bound M and N electrons of the Fe atom are either taken from empirical expressions [24] or from Brinkman and Kramers (BK) estimates [25]. The iron M shell (3d subshell) contains the ferromagnetic polarization. In this polarized electron capture (PEC) model the polarization is thus transferred from the ferromagnetic host exclusively by the capture process.

The maximum field for a certain s-shell is obtained at $\sigma_C = \sigma_L$, i.e. y = 0.5; see (4.1). Since in Fe on the average 2.2 electrons per atom are polarized and only capture from M and N shells into the ion is likely, a maximum of only 7 % of the moving ions can have a polarized unpaired electron.

Although the PEC model was successful in explaining semi-quantitatively the experimental observations [8] several problems remained. The most important one is that for ^{28}Si in Fe at $v > 3v_0$ the tran-

sient field should predominantly be due to unpaired polarized 1s electrons since otherwise one would have an unreasonably high (see above) fraction of ions with polarized 2s electrons. Because of a mismatch of the electron orbital velocities in the Fe 3d and Si 1s shells, capture of 3d electrons into the 1s shell is, however, rather improbable. This is confirmed by BK calculations, which show that capture of (unpolarized) L-electrons dominates. Another problem is encountered in the impossibility to reproduce the general linear velocity dependence of the transient field. This could only be achieved for most nuclides individually by slight adjustment of the BK estimates. This may not be so surprising since it would be rather unlikely that the overlap of two independent and complicated processes would always yield a simple linear relation.

It is clear that in the PEC model the linear v-dependence can only hold to a certain maximum velocity. As the velocity increases the loss cross section for the 1s ionic shell will be increasingly higher than the cross section for capture into this shell. Thus the maximum velocity is estimated to be $v_{max} \leq Zv_o$ according to the Bohr velocity matching principle. A decrease of the transient field was indeed observed for ^{12}C in Fe for $v > 4v_o$ [18] and possibly also for ^{13}C [26] and ^{16}O [27] at high velocities. All other presently available TF-IMPAC integral precession data were obtained at velocities well below this maximum. They are consistent with a linear velocity dependence.

4.2. THE Z-DEPENDENCE

The atomic number dependence in iron was also investigated within the PEC model. No more than a qualitative account of the experimental findings could be obtained, however. To illustrate this we have plotted in fig. 3, for an ion velocity of $v = 4v_o$ the BEA loss cross section and the BK capture cross sections for M and L electrons of iron as a function of the orbital velocity v_f in the moving ion. The orbital velocities for the 1s and 2s shells for various ions are also indicated. For $v_f < 7v_o$ the loss and M-capture cross sections are comparable, yielding $y \approx 0.5$. For $v_f > 9v_o$ the cross sections differ largely, i.e. $y << 0.5$. This indicates that indeed for Z = 6-8 the transient field is mainly due to 1s polarized electrons and for

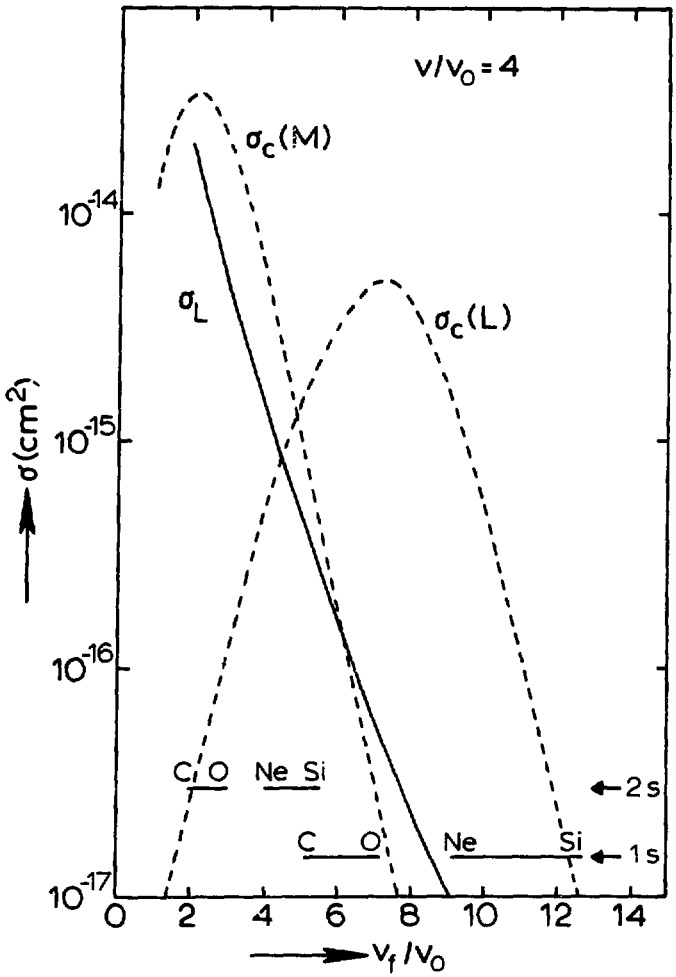

Fig. 3. Electron capture and loss cross sections for ions at $v = 4v_0$ in iron as a function of the orbital electron velocity v_f in the moving ion. For capture the contributions from M and L electrons in iron are given separately. The electron velocities for 1s and 2s shells are indicated for various ions.

Z = 10-14 to 2s polarized electrons. Similarly for Fe one finds that mainly the 3s subshell can contribute.

Apart from the fact that already for $v_f > 5v_0$ capture from the (non-polarized) L-shell dominates there are two severe short-comings in this description. Firstly, the sharp switch from a 1s to a 2s field near Z = 9 is not reproduced and, secondly, the (2s) field strengths at high velocity for Z = 10-14 are difficult to understand. For 2s fields to become sufficiently strong one would have

an average fraction of 30 % of the ions with polarized unpaired 2s electrons at $v \approx 7v_0$. This problem was originally circumvented (see subsect. 4.1) by the assumption that for high v also polarized 1s electrons or possibly $(1s)^1(2s)^1$ configurations with the 2s electron polarized contribute. This would imply, however, that both the strict linear velocity dependence and the observed atomic shell structure are mere accidents.

From this discussion we conclude that in the atomic description another, possibly simpler, mechanism is responsible for the transient magnetic field. It may be that a more direct coupling between the iron 3d subshell and the s-shells of the moving ion governs the ionic polarization. This modification will be discussed in the following.

For light ions at relatively low velocity it is likely that during the collision with an Fe atom a quasimolecule is formed provided that the ion-atom encounter is adiabatic [23]. In such an encounter

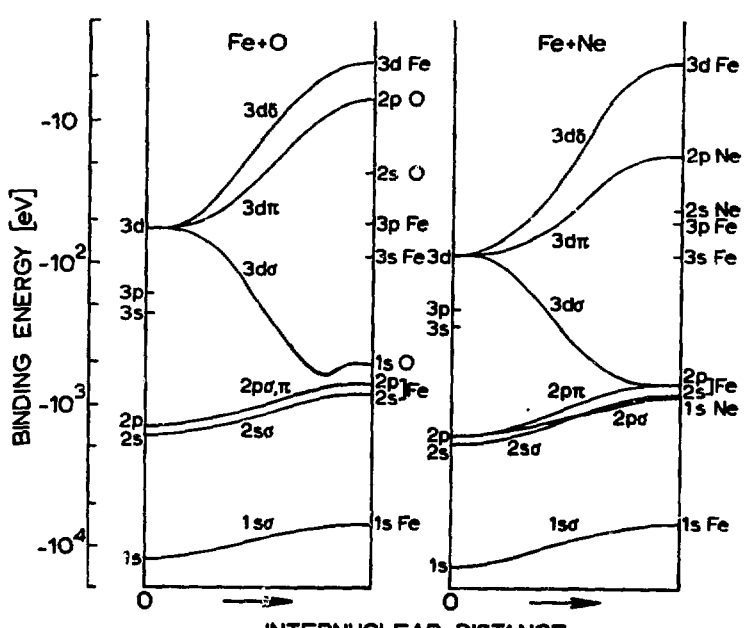

Fig. 4. Schematic representation of the molecular orbital correlation diagrams for the asymmetric diatomic systems Fe + O and Fe + Ne for neutral atoms.

the electron orbits of the collision partners adjust via molecular orbitals (MO) to the molecular orbits. This MO picture had been included already in the PEC model for light ions ($Z \leq 8$) to account for large loss cross sections. We will show that it also leads to a direct coupling of, in particular, the ionic 1s shell and the 3d subshell of the iron host.

In fig. 4 the MO correlation diagram for the Fe + O and Fe + Ne systems are shown. For coupling rules and notation the reader is referred to [23]. For ions with $Z \leq 8$ the diagram is similar to that of Fe + O, whereas for $Z \geq 10$ it is like that of Fe + Ne. Hence for atomic numbers $Z \leq 8$ the ionic 1s orbit couples to the 3d orbit in the united atom thereby considerably reducing the electron binding energy. Therefore an ionic 1s electron is easily lost in the collision. The 3d subshell of iron, which carries the polarization, is also coupled to the 3d orbit of the quasimolecule. During the collision (at closest approach) there is a strong coupling between the two orbitals to the 3d level of the quasimolecule. This direct coupling of the ionic 1s shell to the 3d subshell of iron leads to polarization of the ionic 1s shell. This is so because preferably spin-down electrons can be put in the 3d shell of iron, thereby leaving an unpaired spin-up electron in the ionic 1s shell. For atomic numbers $Z \geq 10$ the ionic 1s electrons are more tightly bound than the 2p electrons of iron and hence the coupling scheme changes drastically. In this case the 1s orbit couples to the deeply bound 2p orbit in the quasimolecule. Consequently no loss of 1s electrons occurs and also polarization of the ionic 1s shell is impossible. Similarly one may have such a step for ionic 2s electrons around $Z = 26$ (Fe). This description shows qualitatively that steps in the transient field strength in iron as a function of Z may be expected at Z-values where indeed such steps have been observed (see fig. 2). These steps are due to switches from primarily 1s to 2s and to 3s fields.

The experimental evidence together with the description in terms of a microscopic model clearly indicates the atomic nature of the transient field in iron, at least for light ions. Additional evidence was obtained very recently [28] in an investigation of the

transient field on ^{19}F in magnetized Fe and Co. The field in Co was found to be substantially stronger than that in Fe, whereas for ^{28}Si in Fe and Co it was found that these fields scale with the polarized electron density of the host (i.e. the Co field is somewhat weaker than the Fe field). The step in the field strength by changing the host atomic number also follows from the MO picture. It has to do with the energy separation of the ionic 1s and host 2p levels. For Fe + F this separation is almost zero, whereas for Co + F it amounts to 100 eV. In the case of small separation the polarization is transferred by a strong radial coupling to the host 2p level.

5. Conclusions and summary

The experimental data, the empirical description and the microscopic interpretation lead to two main conclusions.

(i) The transient field in Fe is well calibrated for light ions ($Z \lesssim 20$).

(ii) There is good evidence for the atomic nature of the transient magnetic field, at least for light ions.

The first conclusion will be briefly discussed in subsect. 5.1 along with a reinterpretation of some earlier g-factor measurements mainly carried out in this laboratory. The second conclusion, which is summarized in subsect. 5.2, leaves still many open questions that have to be answered in the future.

5.1. g-FACTOR MEASUREMENTS

The empirical relation for the v and Z dependence of the transient field in Fe for light ions enables one to perform TF-IMPAC g-factor measurements on short-lived (τ_m = 0.1 - 10 ps) excited nuclear states. This will be shown for ^{32}S and ^{34}S in the next chapter. For heavier ions and other ferromagnetic hosts one may expect that only few calibration experiments suffice to pin down the field strength for these regions. For Gd such a calibration is readily available [16] and has led to recent g-factor measurements on the first-excited 2^+ states of $^{50,54}Cr$, ^{54}Fe and ^{70}Ge recoiling into

Gd [16]. In Fe measurements on the 2_1^+ levels of $^{54,58}Fe$ and $^{58,60,62,64}Ni$ were recently reported [29, 15].

We like to present here also the results of a reinterpretation of previously obtained integral precession data on ^{15}N, ^{26}Mg and ^{30}Si [6, 2, 30]. The values for the g-factors, which were extracted from the data with the presently deduced empirical calibration of the transient field, are summarized in table 2. Since the resulting g-factors differ only little from those given in the original papers the reader is referred to these for a discussion of the results and a comparison with theoretical predictions. Table 2 also includes the g-factor of the 2_1^+ level in ^{20}Ne of which the absolute value was determined in a deorientation experiment [14]. The transient field measurements (subsect. 2.3) determine the sign of this g-factor unambiguously as positive, in agreement with the systematics and simple relations discussed in chapter I.

Table 2

The g-factors extracted from previous integral precession data with the presently deduced empirical transient field calibration

Nucleus (J^π; E_x MeV ; τ_m[ps])	$\Delta\theta$ [mrad]	g [a)]	Ref.
^{15}N ($5/2^+$; 5.27 ; 2.6)	+5.6 ± 1.4	+1.0 ± 0.3 [b)]	[6]
^{20}Ne (2^+ ; 1.63 ; 1.0)		+0.54 ± 0.04	[14]
^{26}Mg (2^+ ; 1.81 ; 0.73)	+1.7 ± 0.3	+0.90 ± 0.18	[2]
^{30}Si (2^+ ; 2.24 ; 0.35)	+0.9 ± 0.2	+0.37 ± 0.09	[30]

a) The errors reflect the uncertainties in the lifetimes, stopping powers, precession angles and field calibration.

b) Corrected for the static field contribution. The field in Fe was taken four times the field in Ni [31].

5.2. CONCLUDING REMARKS

The linear velocity dependence of the transient magnetic field, which is in contrast to the Lindhard-Winther inverse dependence, has been confirmed by the present experiments. These data, together with previous results, have led to the conclusion that this linear v-dependence is a universal feature of the transient field. It has been shown in the foregoing that the presently available experimental data provide a good calibration of the field in Fe for light nuclei. These data have also contributed to a better interpretation of the transient field phenomenon. Not only can the field in Fe be described as a simple expression with ionic hyperfine fields, it has also been shown that such a description is physically meaningful. There is accumulating evidence for the atomic origin of the transient field. One may, however, still wonder why there is no Lindhard-Winther field. It may be that such fields indeed exist. Their strengths, however, are small compared to the huge atomic fields. In other words, subtraction of a Lindhard-Winther contribution from the observed integral precession angles would not alter the present conclusions.

We have seen that the basic features of the transient field in Fe, reflected in the empirical calibration, can be understood in terms of a microscopic model of polarized electron capture. A detailed calculation in which the capture and loss cross sections are explicitly used can only qualitatively account for the observed effects. The sharp structure of the Z-dependence, an atomic shell effect, can only be accounted for by molecular orbital correlation diagrams describing the atomic collision of the moving ion with a host atom. In such a scheme specific ionic s-shells are directly coupled to the 3d subshell of Fe, which carries the polarization. This may explain the necessary very high fraction of ions with an unpaired electron in e.g. the 2s shell (see subsect. 4.2). It may be that the frequency of encounters, which lead to molecular orbital formation, governs the field strength. In that case the dependence of the field on the polarized electron density as well as the linear velocity dependence can be understood.

References

[1] G.K. Hubler, H.W. Kugel and D.E. Murnick, Phys. Rev. Lett. 29 (1972) 622 and Phys. Rev. C9 (1974) 1954

[2] J.L. Eberhardt, R.E. Horstman, H.W. Heeman and G. Van Middelkoop, Nucl. Phys. A229 (1974) 162

[3] J. Lindhard and A. Winther, Nucl. Phys. A166 (1971) 413

[4] G.K. Hubler, Ph. D. thesis, Rutgers University, 1972

[5] G.M. Heestand, P. Hvelplund, B. Skaali and B. Herskind, Phys. Rev. B2 (1970) 3698

[6] M. Forterre, J. Gerber, J.P. Vivien, M.B. Goldberg, K.-H. Speidel and P.N. Tandon, Phys. Rev. C11 (1975) 1976

[7] M. Forterre, J. Gerber, J.P. Vivien, M.B. Goldberg and K.-H. Speidel, Phys. Lett. 55B (1975) 56;
J.F.A. Van Hienen, Ph. D. thesis, Utrecht University, 1975

[8] J.L. Eberhardt, G. Van Middelkoop, R.E. Horstman and H.A. Doubt, Phys. Lett. 56B (1975) 329;
J.L. Eberhardt, R.E. Horstman, P.C. Zalm, H.A. Doubt and G. Van Middelkoop, Hyp. Int. 3 (1977) 195

[9] M. Hass, J.M. Brennan, H.T. King, T.K. Saylor and R. Kalish, Phys. Rev. C14 (1976) 2119

[10] L.C. Northcliffe and R.F. Schilling, Nucl. Data Tables 7 (1970) 223

[11] D. Ward, J.S. Forster, H.R. Andrews, I. V. Mitchell, G.C. Ball, W.G. Davies and G.J. Costa, AECL-5313 (1976)

[12] J.A.J. Hermans, G.A.P. Engelbertink, L.P. Ekström, H.H. Eggenhuisen and M.A. Van Driel, Nucl. Phys. A284 (1977) 307

[13] S. Kalbitzer, H. Oetzmann, H. Grahmann and A. Feuerstein, Z. Phys. A278 (1976) 223

[14] R.E. Horstman, J.L. Eberhardt, H.A. Doubt, C.M.E. Otten and G. Van Middelkoop, Nucl. Phys. A248 (1975) 291

[15] J.M. Brennan, N. Benczer-Koller, M. Hass and H.T. King, reported at: Hyperfine Interactions IV (Madison, 1977) and to be published.

[16] C. Fahlander, K. Johansson, E. Karlsson and G. Possnert, reported at: Hyperfine Interactions IV (Madison, 1977) and to be published.

[17] R. Kalish, J.L. Eberhardt and K. Dybdal, Phys. Lett. 70B (1977) 31

[18] M. Goldberg, E. Konejung, W. Knauer, G.J. Kumbartzki, P. Meyer and K.-H. Speidel, Phys. Lett. 58A (1976) 269

[19] J. Asher, J.R. Beene, M.A. Grace, W.L. Randolph and D.F.H. Start, J. of Phys. G1 (1975) 415;
J. Asher, M.A. Grace, P.D. Johnson, J.W. Koen, P.M. Rowe and W.L. Randolph, J. of Phys. G2 (1976) 477

[20] H. Kopfermann, Kernmomente (Akademische Verlag, Frankfurt, 1956)

[21] Landolt-Börnstein, Zahlenwerte und Funktionen, Band I, Teil 1 (Springer Verlag, Berlin, 1950)

[22] R.R. Borchers, B. Herskind, J.D. Bronson, L. Grodzins, R. Kalish and D.E. Murnick, Phys. Rev. Lett 20 (1968) 424

[23] J.D. Garcia, R.J. Fortner and T.M. Kavanagh, Revs. Mod. Phys. 45 (1973) 111

[24] H.D. Betz, Revs. Mod. Phys. 44 (1972) 465

[25] F. Bell and H.D. Betz, J. of Phys. B10 (1977) 483

[26] J.L. Eberhardt, private communication
[27] R. Kalish, M. Hass, J.M. Brennan and H.T. King, Nucl. Phys. A276 (1977) 339
[28] G. Van Middelkoop, J.A.G. De Raedt, A. Holthuizen, W.A. Sterrenburg and R. Kalish, submitted to Phys. Rev. Lett.
[29] J.M. Brennan, N. Benczer-Koller, M. Hass and H.T. King, Phys. Rev. C16 (1977) 899
[30] J.L. Eberhardt, R.E. Horstman, H.A. Doubt and G. Van Middelkoop, Nucl. Phys. A244 (1975) 1
[31] H. Hamagaki, K. Nakai, Y. Nojiri, I. Tanihata and K. Sugimoto, Hyp. Int. 2 (1976) 187

CHAPTER V

TRANSIENT FIELD g-FACTOR MEASUREMENTS ON THE 2_1^+ STATES OF ^{32}S AND ^{34}S

1. Introduction

It has been shown in the previous chapter that the transient magnetic field experienced by a nucleus slowing down in polarized Fe can be parametrized as a function of atomic number and recoil velocity of the moving ion. At least for nuclei with $Z \lesssim 20$ the calibration that results from this parametrization is expected to be quite accurate. This enables one to perform g-factor measurements on short-lived (τ_m = 0.1 - 10 ps) excited states by the transient field implantation perturbed angular correlation (TF-IMPAC) technique in this region. In this chapter the above statements will be elucidated by the report of g-factor measurements on the first-excited 2^+ states of ^{32}S and ^{34}S.

The investigation of these even sulphur isotopes is an extension of the series of g-factor measurements on first-excited 2^+ states in selfconjugated (T_3 = 0) and neutron-excess (T_3 = +1) even-even nuclei in the sd shell, Ne, Mg and Si, carried out so far in this laboratory [1]. The lifetimes of these states (0.23 ps for ^{32}S and 0.41 ps for ^{34}S) are also sufficiently short in comparison to the stopping time for initial ion velocities of $v_i/v_o \approx 1.5$ (v_o = c/137), to ensure that the contribution of the (unknown) static field to the measured integral precessions is negligible. Finally the g-factor of ^{32}S is reliably known to be 0.5 to within 10% from systematics as was outlined in chapter I. Hence a TF-IMPAC measurement of this g-factor also provides a test of the transient field calibration as obtained in chapter IV.

2. Experimental procedure

The 2.23 and 2.13 MeV levels of ^{32}S and ^{34}S, respectively, were excited by inelastic scattering of α-particles. The experimental set-up, with a single-crystal Fe window frame as a target backing, has been described in detail in chapter III.

The coincident yields and γ-ray anisotropies for these reactions were first measured as a function of the $^{4}He^{++}$ bombarding energy. Outgoing α-particles were detected at 180° with respect to the beam direction, in coincidence with γ-rays detected in NaI(Tl) counters at 45° and 90°. The bombarding energies ranged from just above the Coulomb barrier (7.5 MeV) to about 12 MeV. Higher energies had to be discarded because of the prolific background due to reactions in the thick iron backing. The optimum α-particle bombarding energies for the integral precession measurements were found to be 8.25 MeV for ^{32}S and 8.90 MeV for ^{34}S. It would have been attractive to use the inverse reactions $^{4}He(S, \alpha)$ at the same centre-of-mass energy. In that case the recoil velocity of the excited S nuclei would have been four times as high as in the (α, α') reactions and consequently the precessions would have been larger by at least the same factor (see chapter IV). Unfortunately the Utrecht 7MV tandem accelerator is not capable to produce a beam of ^{32}S at 65-70 MeV of sufficient intensity.

Targets of about 200 μg/cm^2 ZnS were prepared by vacuum evaporation on the Fe single-crystal frame. The thicknesses were determined both by weighing of a sample which was prepared simultaneously under identical conditions and by comparing the coincident γ-ray yields with those of accurate 600 μg/cm^2 ZnS targets on thin formvar backings. For the ^{32}S experiment a natural ZnS target (i.e. the sulphur is 95% ^{32}S) and for the ^{34}S experiment $Zn^{34}S$ enriched to 90% in ^{34}S were used.

The γ-ray energies corresponding to the first-excited states of ^{32}S and ^{34}S cannot be resolved by the six 12.7 cm diam. by 12.7 cm long NaI(Tl) detectors at angles ±18°, ±72° and ±108°. Therefore a large-volume Ge(Li) detector was positioned at 0° to the beam direction to monitor the relative contribution of ^{32}S coincident γ-rays

in the ^{34}S experiment. This contribution was found to be less than 3%. From the yield measurements it was calculated that in the ^{32}S experiment at E_α = 8.25 MeV the contribution of ^{34}S γ-rays to the photo-peak of the 2.23 MeV γ-ray in ^{32}S was less than 1%.

The single-crystal frame was magnetized by a current of 0.8 A through a 60 turn coil on one of the legs, corresponding to a magnetizing field of about 15 gauss (1200 A/m). The direction of this field was reversed automatically every 2 min. In order to maintain good true-to-random coincidence ratios, to limit pulse pile-up and dead-time losses and to prevent heating of the frame, the beam current (typically 70 nA for ^{32}S and 55 nA for ^{34}S) was not allowed to exceed 80 nA ($^{4}He^{++}$).

The logarithmic derivative $W^{-1}dW/d\theta$ of the γ-ray angular correlation function $W(\theta)$ was determined by off-setting the six-counter array by angles of $\pm 2^{\circ}$ as explained in chapter III. The total background-subtracted yield obtained in the photo-peak for ^{32}S was 2.4 x 10^5 counts per detector for each field direction and 1.4 x 10^5 for ^{34}S. The measurements required a beam time of 100 h each. The quality of the data obtained for e.g. ^{34}S can be inferred from the coincident α-particle, γ-ray and time spectra displayed in fig. 1.

3. Statistical considerations, analysis and results

3.1. STATISTICS

The observed effects ε as well as the cross effects ε_c, defined in chapter III, are summarized in table 1 together with the W^{-1} $dW/d\theta$ calibration. The results for the detector pairs at $\pm 72^{\circ}$ and $\pm 108^{\circ}$ have been averaged. For the detector pair at $\pm 18^{\circ}$ the results are given separately since here the logarithmic derivative of $W(\theta)$ is different from those at $\pm 72^{\circ}$ and $\pm 108^{\circ}$ due to the finite solid angles of the γ-ray counters. For these two counters no cross effects can be given. The mean integral precession angles $\Delta\theta$ deduced from the data are also included in table 1.

Frequency distributions of the effects and cross effects per recorded magnetic tape (70 min for ^{32}S and 100 min for ^{34}S) served as

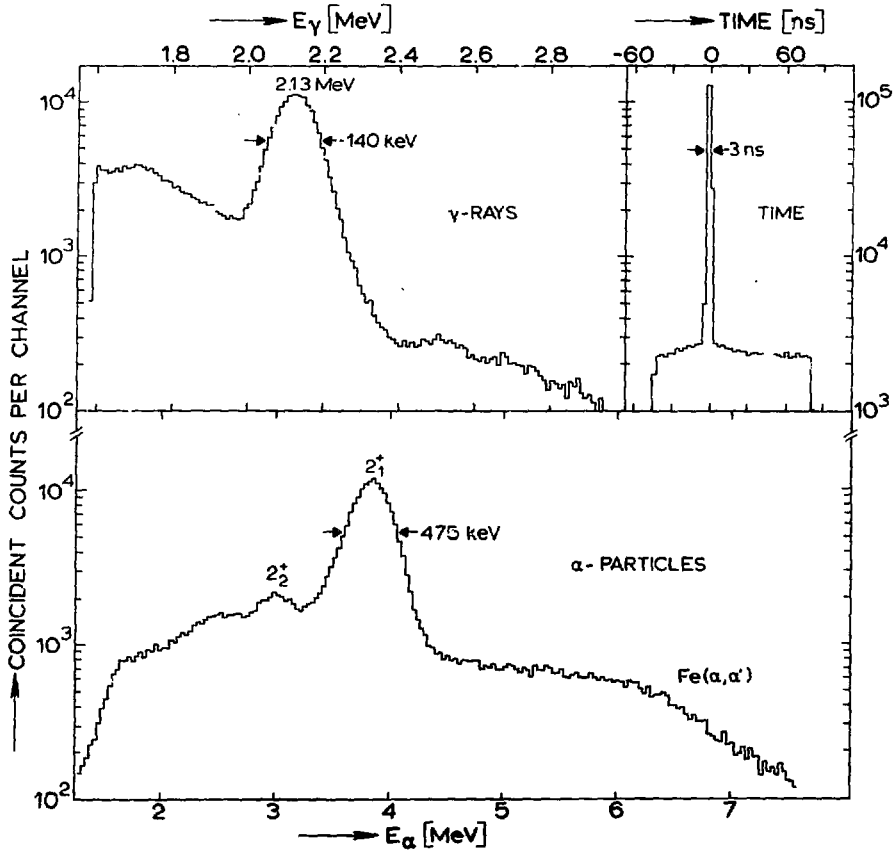

Fig. 1. Typical coincident α-particle, γ-ray and time spectra for ^{34}S. The spectra were generated with windows set on the respective peaks. No random background has been subtracted.

a check on the data. No significant deviations from a Gaussian distribution were observed (see fig. 2). To investigate a possible radiation damage effect and other systematic trends in the measured rotation, the experiments were divided into runs of about 3.5 h and the mean precession angle per run was calculated. The results are displayed in fig. 2. There is no significant decrease of the rotation with time.

3.2. THE g-FACTORS

The experimentally observed integral precession angles were interpreted with the transient field dependence on recoil velocity and atomic number as obtained in chapter IV. The field was assumed to be due to unpaired polarized 2s electrons of the moving ion and is

Table 1

Summary of the measured effects [a] and deduced precessions for ^{32}S and ^{34}S

Nucleus	Precession in Fe		Calibration $\pm 2^{o}$ off-set		$\Delta\theta$ [mrad]
	ε [%]	ε_c [%]	ε [%]	ε_c [%]	
^{32}S	1.69 ± 0.33	-0.16 ± 0.33	79 ± 2	1 ± 2	} 1.06 ± 0.18
	1.70 ± 0.41		67 ± 3		
^{34}S	3.00 ± 0.45	0.20 ± 0.45	73 ± 2	2 ± 3	} 1.80 ± 0.25
	1.92 ± 0.60		54 ± 3		

[a] The results of the detector pairs at $\pm 72^{0}$ and $\pm 108^{o}$ have been averaged.

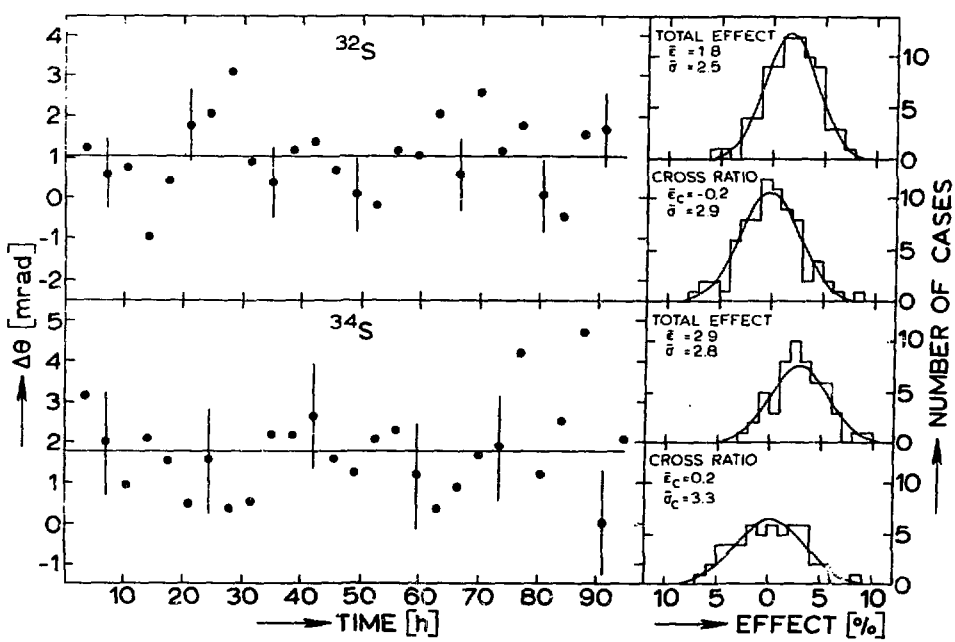

Fig. 2. The measured rotation angles $\Delta\theta$ per run of 3.5 h as a function of time. The solid lines represent the average value. Frequency distributions of the precession effects ε and cross effects ε_c per recorded magnetic tape are also shown. The results of the detector pair at $\pm 18^{o}$ have been scaled by the $W^{-1}dW/d\theta$ calibration and averaged with the results of the pairs at $\pm 72^{o}$ and $\pm 108^{o}$. The expected Gaussian distributions are indicated.

given by $B_{TF} = C(Z=16)v/v_o$. The program FIELD, discussed in chapter IV, was used to deduce the g-factors and also to calculate the error propagation. The resulting relative errors in the g-factors are given in table 2. The contributions of the uncertainties in each quantity to the total error are also shown; they will be discussed in some detail below.

Table 2

Sources of errors and their contribution to the error in the g-factors

Quantity [a]	^{32}S		^{34}S	
	relative error [%]	contribution to g [%]	relative error [%]	contribution to g [%]
$\Delta\theta$	17	17	14	14
B_s	100	0	100	1
τ_m	9	8	10	5
dE/dx	5	2	5	3
d	10	4	10	2
C(16)	4	4	4	4
	total error	20	total error	16

[a] The symbols are explained in the text.

(i) Static field B_s. As mentioned already in the introduction the static field for S in Fe is not known. An estimate may be obtained by taking the systematic trend of the fields in series of elements with similar electron configurations, e.g. In and following elements, and scaling this down to the known fields of the nearby elements Al and P in Fe [2]. This leads to the conclusion that the static field must be smaller in magnitude than 10 T, which gives rise to a correction for ^{34}S of at most 1%. For ^{32}S the static field contribution is even a factor of five smaller.

(ii) Mean lives τ_m. The values for the mean lives of the ^{32}S and

^{34}S first-excited states are 225 ± 20 fs and 410 ± 40 fs, respectively [3]. The sensitivity of the calculated precessions to variations of τ_m is high for lifetimes appreciably shorter than the stopping time, and low to non-existent for lifetimes much longer than the stopping time.

(iii) Stopping power dE/dx. Electronic stopping powers in Fe from the tabulation of Northcliffe and Schilling [4] were scaled by recent data from Ward et al. [4] on the stopping of α-particles as discussed in detail in chapter IV. For the nuclear stopping power the universal function of Kalbitzer et al. [4] was taken. The uncertainty in the electronic stopping powers thus obtained is estimated to be at most 5%. For the nuclear stopping powers an error of 25% was adopted. Even if a 50% uncertainty is assumed, however, the figure in table 1 remains unchanged.

(iv) Target thickness d. The two independent thickness estimates discussed in sect. 2 agree to within 15%, which leads to an estimated uncertainty of about 10%.

(v) Z-dependence of the field C(16). The constant C(Z=16) was computed from the systematics described in chapter IV, sect. 3. This leads to C(16) = 277 ± 11 [T].

The errors are treated independently and yield relative errors in the values of the g-factors for ^{32}S and ^{34}S of 20% and 16%, respectively. This leads to the final results for $^{32}S(2_1^+)$ and $^{34}S(2_1^+)$ of g = +0.47 ± 0.09 and g = +0.51 ± 0.08, respectively.

4. Comparison with theory and conclusion

The experimental values for the g-factors of the first-excited 2^+ states of ^{32}S and ^{34}S are compared with some theoretical predictions in table 3. The calculations are specified in some detail below.

(i) PHF. A projected Hartree-Fock calculation with the lowest five major oscillator shells as model space [5].

(ii) MSDI. A shell-model calculation [6] in a $1d_{5/2}2s_{1/2}1d_{3/2}$ configuration space with up to two holes in the $1d_{5/2}$ orbit. The modified surface-delta interaction is taken as effective two-body inter-

Table 3

Comparison of theoretical g-factors with experiment

		^{32}S	^{34}S
Experiment		+0.47 ± 0.09	+0.51 ± 0.08
Theory [a]:	PHF [b]	+0.53	
	MSDI [c]	+0.51	+0.54
	ASDI [d]	+0.49	
	CW [e]	+0.50; +0.53	+0.43; +0.50
	pure $s_{1/2}^{-1}d_{3/2}$	+0.54	
	Z/A	+0.50	+0.47

[a] The abbrevations are explained in the text.
[b] Ref.[5]; [c] Ref.[6]; [d] Ref.[7].
[e] Ref.[8], the first and second value correspond to calculations with bare and effective nucleon g-factors, respectively.

action.

(iii) ASDI. An sd shell-model calculation [7] with an "adjusted surface-delta interaction". The configuration space is truncated with the diagonal energy truncation method.

(iv) CW. A full sd-space shell-model calculation by Chung and Wildenthal [8]. The 63 two-body matrix elements and 3 single-particle orbital energies were fitted to low-lying positive parity levels in A = 32-39 nuclei. Results with bare and effective single-particle spin and orbital g-factors are given. The latter allegedly should give better agreement.

For the sake of completeness also the pure $2s_{1/2}^{-1}1d_{3/2}$ estimate for ^{32}S (see chapter I, subsect. 4.1) is included. The rotational model estimates g = Z/A are indicated, since it was shown in chapter II that the static quadrupole moments of the 2_1^+ states in ^{32}S and ^{34}S can be explained within the framework of such a model.

As pointed out in detail in Chapter I the g-factors of low-lying

states of selfconjugated even-even nuclei are close to g = 0.5. They are not sensitive to the interaction used nor to the size of the configuration space as is again clearly demonstrated for ^{32}S. On the other hand, however, also the theoretical estimates for ^{34}S show very little spread. All calculations predict a vanishing isovector part of the g-factor. It is generally found that the isovector g-factors are small in the $1d_{3/2}$ subshell (see chapter I).

In conclusion it may be stated that the mutual agreement of the theoretical predictions as well as the good agreement with the g-factors deduced from the experimental data provides confidence in the calibration of the dependence of the transient field in Fe on velocity and atomic number.

References

[1] J.L. Eberhardt, R.E. Horstman, H.W. Heeman and G. van Middelkoop, Nucl. Phys. A229 (1974) 162;
J.L. Eberhardt, R.E. Horstman, H.A. Doubt and G. van Middelkoop, Nucl. Phys. A244 (1975) 1;
R.E. Horstman, J.L. Eberhardt, H.A. Doubt, C.M.E. Otten and G. van Middelkoop, Nucl. Phys. A248 (1975) 291;
R.E. Horstman, J.L. Eberhardt, P.C. Zalm, H.A. Doubt and G. van Middelkoop, Nucl. Phys. A275 (1977) 237

[2] G.N. Rao, Atomic and Nucl. Data 15 (1975) 553

[3] P.M. Endt and C. van der Leun, Nucl. Phys. A214 (1973) 1

[4] L.C. Northcliffe and R.F. Schilling, Nucl. Data Tables 7 (1970) 223;
D. Ward, J.S. Forster, H.R. Andrews, I.V. Mitchell, G.C. Ball, W.G. Davies and G.J. Costa, AECL-5313 (1976);
S. Kalbitzer, H. Oetzmann, H. Grahmann and A. Feuerstein, Z. Phys. A278 (1976) 223

[5] M.R. Gunye, Phys. Lett. 37B (1971) 125

[6] P.W.M. Glaudemans, P.M. Endt and A.E.L. Dieperink, Ann. of Phys. 63 (1971) 134

[7] F.E.H. van Eijkern, G.A. Timmer, F. Meurders and P.W.M. Glaudemans, Z. Phys. A278 (1976) 337

[8] W. Chung and B.H. Wildenthal, to be published;
W. Chung, Ph.D. thesis, Michigan State University, 1976.

SAMENVATTING

In dit proefschrift wordt theoretisch en experimenteel onderzoek aan statische kernmomenten beschreven. In het eerste deel worden enkele eenvoudige theoretische relaties voor magnetische dipool- en electrische quadrupoolmomenten afgeleid en besproken. In het tweede deel komt een experimentele methode voor het meten van magnetische dipoolmomenten van kortlevende kerntoestanden aan de orde. De inhoud van elk der hoofdstukken wordt hieronder kort weergegeven.

Hoofdstuk I. Hierin worden magnetische dipoolmomenten bestudeerd waarbij wordt uitgegaan van het schillenmodel. Eerst wordt een optelrelatie voor dipoolmomenten van nabuurkernen besproken. Vervolgens wordt voor lichte kernen de splitsing van het dipoolmoment in een isoscalair en een isovector deel bekeken. Daar, waar de gevonden uitdrukkingen ongevoelig blijken voor de details van de golffunctie, wordt een afschatting gegeven met de veronderstelling dat alle actieve kerndeeltjes zich in dezelfde subschil bevinden. Verder wordt gebruik gemaakt van matrixelementen verkregen uit gegevens over β-verval. Alle gevonden relaties worden waar mogelijk getoetst aan experimentele resultaten. Deze vergelijking levert een goede overeenstemming op.

Hoofdstuk II. In dit hoofdstuk wordt een relatie afgeleid voor electrische quadrupoolmomenten van rotatietoestanden in kernen met even aantallen protonen en neutronen. Hierbij wordt uitgegaan van een model waarbij de kern bestaat uit een superfluïde romp en een zich collectief daaromheen bewegende stroom deeltjes. Onder bepaalde veronderstellingen legt de gevonden relatie een, in eerste orde lineair, verband tussen het quadrupoolmoment en de excitatie-energie van een kerntoestand. Vergelijking van voorspelde quadrupoolmomenten met experimenteel gevonden resultaten laat een zeer goede overeenstemming zien. Ook wordt het gevonden verband vergeleken met relaties afgeleid voor quadrupoolmomenten bepaald uit sterkten van γ-overgangen tussen rotatietoestanden.

Hoofdstuk III. Hierin komt de stootveldmethode voor het meten van magnetische dipoolmomenten aan de orde. Het magnetische stootveld wordt ondervonden door een kern tijdens zijn afremming in ge-

polariseerde ferromagnetica. Ten gevolge van de wisselwerking tussen dit veld en het dipoolmoment van een aangeslagen kerntoestand gaat de kern precederen. Deze precessie wordt gemeten als een verdraaiing van de intensiteitsverdeling van de bij verval uitgezonden γ-straling. Bij gebruik van een éénkristallijn ijzerraampje als trefplaatdrager blijkt dat een winst in meettijd van tenminste een factor vier ten opzichte van de conventionele methode wordt bereikt. De goede werking van deze nieuwe opzet wordt aangetoond door magnetisatiemetingen en door vergelijking voor enkele gevallen met de conventionele methode.

Hoofdstuk IV. In dit hoofdstuk wordt het stootveld in gemagnetiseerd ijzer bestudeerd aan de hand van een aantal precessiemetingen aan ^{20}Ne en ^{24}Mg. Ook elders gevonden resultaten worden hierbij betrokken. De eerder gevonden lineaire afhankelijkheid van het stootveld van de snelheid van de kern wordt bevestigd. Uit deze metingen volgt ook een zeer markante afhankelijkheid van het atoomgetal van de bewegende kern. Dit gedrag kan begrepen worden door aan te nemen dat het stootveld wordt veroorzaakt door ongepaarde en gepolariseerde electronen in s-banen van het ion van de kern. Een qualitatieve verklaring van deze empirische beschrijving blijkt mogelijk binnen een microscopisch model waarbij gepolariseerde electronen uit het ijzer in de betrokken s-banen van het bewegend ion worden gevangen. De gevonden scherpe "zaagtandachtige" afhankelijkheid van het atoomgetal kan worden begrepen als in de atomaire botsingen tussen het ion en ijzeratomen quasimoleculen worden gevormd.

Hoofdstuk V. Tenslotte wordt in dit hoofdstuk de gevonden empirische calibratie van het stootveld in ijzer gebruikt om de dipoolmomenten te meten van de eerste aangeslagen toestanden van ^{32}S en ^{34}S. De gevonden waarden komen goed overeen met theoretische voorspellingen, waaronder die op basis van de relaties afgeleid in hoofdstuk I.

CURRICULUM VITAE

De schrijver van dit proefschrift werd op 16 januari 1951 te Eindhoven geboren. Na het behalen van het diploma HBS-B aan het "Lorentz Lyceum" aldaar, begon hij met zijn studie aan de Rijksuniversiteit te Utrecht (1968).

Het kandidaatsexamen wis- en natuurkunde legde hij af in maart 1971. In juli 1973 werd het doctoraalexamen (toegepaste) wiskunde met bijvak theoretische natuurkunde afgelegd. Daarna volgde in juli 1974 het doctoraalexamen (experimentele) natuurkunde met bijvakken zuivere wiskunde en toegepaste psychologie (cum laude). Het "groot onderzoek" werd verricht in de Utrechtse werkgroep kernfysica en heeft ten dele geleid tot hoofdstuk I van dit proefschrift.

Vanaf juli 1974 is hij werkzaam bij dezelfde werkgroep als wetenschappelijk medewerker van de Stichting voor Fundamenteel Onderzoek der Materie. Naast zijn onderzoek gaf hij werkcolleges natuurkunde aan voor-kandidaats studenten.

Door de Stichting voor Fundamenteel Onderzoek der Materie werd hij in de gelegenheid gesteld om in 1976 de "Workshop on Topics in Atomic Physics Related to Nuclear Experimentation" te Haifa en in 1977 de Zomerschool (Nuclear Spectroscopy) te Nijenrode te bezoeken.

Stellingen behorende bij het proefschrift

A STUDY OF THE TRANSIENT MAGNETIC FIELD IN IRON
AND SIMPLE RELATIONS FOR NUCLEAR MOMENTS

1. In de zend-ontvangst karakteristiek van tunneldioden met gap Δ is, bij voldoend hoge injectiestromen, niet alleen bij $eV = 4\Delta$, maar ook bij $eV = 3\Delta$ een knik te verwachten.
W. Eisenmenger and A.H. Dayem, Phys. Rev. Lett. 18 *(1967) 125.*

2. In zijn analyse van de door Liang en Joshi gemeten ionengeleiding van zuiver β-PbF_2, gaat Kennedy voorbij aan de mogelijkheid dat anion vacatures verantwoordelijk kunnen zijn voor deze geleiding.
C.C. Liang and A.V. Joshi, J. Electrochem. Soc. 122 *(1975) 466;*
J.H. Kennedy, ibid., 122 *(1975) 1641.*

3. Ten onrechte concludeert Forman uit oppervlakteanalyse met behulp van Augerspectroscopie, dat op het oppervlak van een geïmpregneerde kathode niet aan zuurstof gebonden barium naast niet aan barium gebonden zuurstof voorkomt.
R. Forman, J. Appl. Phys. 47 *(1976) 5272.*

4. De opvatting dat de eigenschappen van een oxidekathode bepaald worden door zijn poreuze structuur, is niet voor bestrijding vatbaar. De door Soukup ten gunste van dit model aangevoerde argumenten zijn echter onjuist.
R.J. Soukup, J. Appl. Phys. 48 (1977) 1098.

5. Het bewijs van het definiet niet-negatief zijn van Kullback's informatiemaat kan eleganter en korter geformuleerd worden.
S. Kullback, Information Theory and Statistics (Dover Publ. Inc., New York, 1968).

6. Bij onderzoek aan instabiliteiten in toroïdale plasmastromen kan het nut van spoeltjes, die de poloïdale component van het daarbij optredende magneetveld meten, betwijfeld worden.
P.C. Zalm, Intern rapport 74/020 FOM Instituut voor Plasmafysica, Utrecht.

7. De aanpassing van de oppervlaktedeltawisselwerking door Meurders en anderen draagt niet bij tot het verkrijgen van inzicht in de rol van de effectieve wisselwerking in schillenmodelberekeningen.
P. Meurders et al., Z. Phys. A276 (1976) 113;
P.E.H. van Eijkern et al., Z. Phys. A278 (1976) 337.
J.E. Koops and P.W.M. Glaudemans, Z. Phys. A280 (1976) 181.

8. Bij stootveldmetingen heeft het gebruik van éénkristallijne ijzerraampjes die enkele gewichtsprocenten silicium bevatten, voordelen boven raampjes vervaardigd uit zuiver ijzer.
Hoofdstuk III van dit proefschrift.

9. Bij de behandeling van hypertrofische pylorusstenose bij pasgeborenen, moet bij twijfel altijd de voorkeur gegeven worden aan de operatieve therapie boven de conservatieve therapie.
E.W. Boeschoten, J.A. Taminiau en P.C. Zalm, te publiceren.

10. Ondanks het feit dat het Braille-schrift algemeen aanvaard is, dient de efficiëntie ervan aan een ergonomisch onderzoek onderworpen te worden.
P.C. Zalm, Rapport 74-6 Psychologisch Laboratorium, Rijksuniversiteit Utrecht.

11. Bij het intrappen van open deuren dient men voldoende stoplappen achter de hand te houden om te voorkomen dat men zelf op de tocht komt te staan.

12. Menig experimenteel fysicus is slechts theoretisch fysicus.

P.C. Zalm 30 november 1977